

# Development of structural correlations and synchronization from adaptive rewiring in networks of Kuramoto oscillators

Lia Papadopoulos,<sup>1</sup> Jason Kim,<sup>2</sup> Jürgen Kurths,<sup>3,4,5</sup> and Danielle S. Bassett<sup>2,6</sup>

<sup>1</sup>*Department of Physics and Astronomy, University of Pennsylvania, Pennsylvania, PA 19104, USA*

<sup>2</sup>*Department of Bioengineering, University of Pennsylvania, Pennsylvania, PA 19104, USA*

<sup>3</sup>*Potsdam Institute for Climate Impact Research - Telegraphenberg A 31, 14473 Potsdam, Germany*

<sup>4</sup>*Department of Physics, Humboldt University Berlin - 12489 Berlin, Germany*

<sup>5</sup>*Institute for Complex Systems and Mathematical Biology,  
University of Aberdeen - Aberdeen AB24 3UE, UK*

<sup>6</sup>*Department of Electrical & Systems Engineering,  
University of Pennsylvania, Pennsylvania, PA 19104, USA\**

(Dated: July 25, 2022)

Synchronization of non-identical oscillators coupled through complex networks is an important example of collective behavior, and it is interesting to ask how the structural organization of network interactions influences this process. Several studies have explored and uncovered optimal topologies for synchronization by making purposeful alterations to a network. On the other hand, the connectivity patterns of many natural systems are often not static, but are rather modulated over time according to their dynamics. However, this co-evolution - and the extent to which the dynamics of the individual units can shape the organization of the network itself - are less well understood. Here, we study initially randomly connected but locally adaptive networks of Kuramoto oscillators. In particular, the system employs a co-evolutionary rewiring strategy that depends only on instantaneous, pairwise phase differences of neighboring oscillators, and that conserves the total number of edges, allowing the effects of local reorganization to be isolated. We find that a simple regulatory rule - which preserves connections between more out-of-phase oscillators while rewiring connections between more in-phase oscillators - can cause initially disordered networks to organize into more structured topologies that support enhanced synchronization dynamics. We examine how this process unfolds over time, finding both a dependence on the intrinsic frequencies of the oscillators and the global coupling, in terms of how the adaptive mechanism reorganizes the network and influences the dynamics. Importantly, for large enough coupling and after sufficient adaptation, the resulting networks exhibit interesting characteristics, including degree - frequency and frequency - neighbor frequency correlations. These properties have previously been associated with optimal synchronization or explosive transitions in which the networks were constructed using global information. On the contrary, by considering a time-dependent interplay between structure and dynamics, this work offers a mechanism through which emergent phenomena and organization can arise in complex systems utilizing local rules.

Electrical activity in populations of neurons, or the spread of information or disease across social networks are common examples of dynamical processes unfolding on networks. In many real-world systems, synchronization of dynamics, and its dependence on network architecture, is of critical interest. Importantly, these network interactions can also be adaptive, such that connections rearrange over time according to the dynamical states of the nodes. A prevalent example of this takes place in biological neuronal networks, which reconfigure via local plasticity mechanisms that are informed by the dynamical relationships between directly coupled elements. Motivated by such systems, here we address the question of how both structured network topology and global synchronization can develop through a co-evolution of the underlying network connectivity and the dynamics. Using the canonical Kuramoto

model, we suggest a simple, adaptive rewiring scheme based on local phase information that can evolve initially unstructured random graphs towards topologies with specific organizational principles. In turn, we find that this process simultaneously enhances synchronization. The structure that arises in the co-evolving systems manifests as certain couplings between the natural frequencies of the oscillators and the network topology, properties that have previously been associated with optimal synchronization in which the networks were purposefully constructed using complete information of the network and node properties. Yet here, without any global information, we consider a time-dependent interplay between structure and dynamics, and offer a mechanism through which organization can emerge in complex systems utilizing local rules.

---

\* dsb@seas.upenn.edu

## I. INTRODUCTION

Exactly how dynamical processes unfold on networks with non-trivial coupling between individual units remains an important question in complex systems science [1–4]. Examples of such dynamical systems on networks include the time-dependent patterns of electrical activity in populations of neurons [5–11], the spread of information or disease across social networks [12–15], or regulatory mechanisms in biological networks [16–20]. In each case, the way the system evolves over time is dependent on the specific form of the dynamics, intrinsic properties of each element (either of nodes or edges), and the architecture of connectivity. Intriguing questions are if and how collective behavior can emerge in these complex, heterogeneous systems. A significant and widespread manifestation of such collective behavior is synchronization [21–25], in which a group of interacting elements converge to the same state or evolve in unison over time. Real-world illustrations of this phenomenon range from circadian clock cycles [22, 26], to the rhythmic patterns of functional activity in the human brain [27–38], and synchronization in power-grid networks [39–42].

One of the most common and useful models for studying synchronization is the canonical Kuramoto model [43, 44], which originally described the evolution of a population of  $N$  all-to-all coupled phase oscillators that were in general non-identical (see [45, 46] for reviews). In recent years, this model has been extended to study systems with heterogeneous network topologies, in order to investigate how the architecture of complex connectivity affects the onset of synchronization in diverse oscillator populations [25, 47]. Such efforts have provided important insights into the nature of the synchronization transition in different graph models including those that display a scale-free degree distribution [48–52], those with small-world architecture [53, 54], and those with community structure [55–61].

Within this body of work, particular attention has been paid to understanding what features of a network inhibit or enhance the ability to support collective dynamics. For the case of identical oscillators, this is often studied from the perspective of minimizing a ratio of eigenvalues – the eigenratio – that depends only on the structure of the network [62, 63]. However, the question of “optimal” networks for synchronization is more interesting and complex when the oscillators’ natural frequencies are heterogeneous, a characteristic of many real-world systems. In particular, for non-identical oscillators, a crucial consideration becomes how the structure of the network is intertwined with dynamical properties. For example, in the Kuramoto model, synchronization can be enhanced when there are specific types of correlations between node degrees and oscillator frequencies or between the natural frequencies of adjacent oscillators [64, 65]. Gómez-Gardeñes *et al.* [66] demonstrated that in scale-free networks, positive frequency-degree correlations can lead to a first-order, or explosive, transition

to synchronization. More recently, discontinuous transitions have been found by imposing constraints on the minimal difference between connected nodes’ natural frequencies [67, 68]. There has also been analytical progress in determining network topologies that enhance synchronization. For example, it has been shown that optimal networks for synchronizing collections of non-identical oscillators exhibit particular relationships between Laplacian eigenvectors and node frequencies [69–71]. In addition, dimensional reduction approaches [72] have recovered many previous numerical results, and have been used to derive analytical conditions for optimizing synchronization of Kuramoto oscillators in networks with attractive and repulsive interactions [73].

Notably, while the coupling structure between oscillators can drive their dynamics, network dynamics can also modulate structure. Specifically, in adaptive systems, the pattern of connectivity itself is continuously updated and modified in response to the dynamics that occur on top of it [74–76]. Systems that display these processes can be observed across biological, ecological, social, and distribution networks [74, 75], and collectively they can be characterized by topology and dynamical states that co-evolve with one another. Kuramoto-like models in particular provide a useful framework in which to explore the effects of co-evolution and adaptation [77–89], and allow one to address questions such as *(i)* can and how might these systems self-organize towards a network configuration that enhances local or global synchronization?, and *(ii)* from an initially unstructured topology, how do different adaptive mechanisms lead to the emergence of certain organized architectural patterns or correlations between dynamical properties and network structure?

In addition to being adaptive, it is important to note that the evolution of many real-world networks is often governed by *local* rules, in which node dynamics update as a function of only neighboring node states, and in turn, the placement or weights of edges update primarily as a function of the states of the nodes they directly couple [74–76]. This type of behavior is especially pertinent in biological systems, which typically co-evolve in the absence of global or top-down controllers of node states and/or network structure. A particularly salient example of this occurs in biological neuronal networks, where, under Hebbian plasticity rules, increases in synaptic weights occur when connected neurons exhibit correlated dynamics [90–92], while under anti-Hebbian plasticity rules, the opposite occurs [93, 94]. Other systems that obey such local adaptation are prevalent, and studied examples include models of reconfiguration of social networks under disease propagation [95] and opinion formation [96], or reorganization under feedback mechanisms in boolean models with applications to gene regulatory or neural networks [97, 98].

In this study, we use the Kuramoto model to investigate how a simple, adaptive rewiring scheme can evolve initially unstructured random graphs towards ordered topologies, and also simultaneously lead to enhanced syn-

chronization in the system. Importantly, the rule is informed by only local information of neighboring nodes' states at a given instant of time, and works by regularly breaking and randomly rewiring connections between more instantaneously phase-synchronized oscillators, while maintaining connections between more desynchronized pairs of oscillators. This process repeats continually over time, and can be thought of as a repulsive mechanism, or one that tends to repress assortativity (in terms of nodes connecting to other nodes with similar instantaneous phases). We find that co-evolution of the network and dynamics can promote the degree of synchronization in the system, which occurs in tandem with the development of organized structure in the network in the form of specific correlations between the topology and natural frequencies. In previous work, these features have been imposed by purposeful selection, or have been shown to arise in work on optimizing synchronization. Here, however, the results constitute emergent phenomena. Focusing on the simplest situation of binary, undirected networks, we isolate the effects of adaptive reconfiguration alone, and thereby uncover a self-regulatory process through which heightened collective dynamics and organized network structure simultaneously arise in a local, unsupervised way.

The remainder of this paper is organized as follows. Sec. II states the formulation of Kuramoto dynamics on complex networks. In Sec. III we first briefly outline past work to motivate the specific mechanism studied here, and then detail the proposed co-evolutionary strategy. Sec. IV describes several interesting results of the adaptive process, and in Sec. V we discuss the implications of our findings and conclude.

## II. THE KURAMOTO MODEL ON COMPLEX NETWORKS

Of the many models that exist for studying synchronization phenomena on complex networks, one of the most useful has been the paradigmatic Kuramoto model [43, 44]. It describes the dynamical evolution of a population of  $N$  phase oscillators coupled on a network according to the following equation:

$$\dot{\theta}_i = \omega_i + \alpha \sum_{j=1}^N A_{ij} \sin(\theta_j - \theta_i). \quad (1)$$

In this formulation,  $\theta_i$  is the instantaneous phase of the  $i^{\text{th}}$  oscillator,  $\omega_i$  is its natural frequency,  $\alpha$  is the overall coupling strength, and  $\mathbf{A}$  is the  $N \times N$  adjacency matrix describing the connectivity of the network. In this report, we consider binary, undirected networks, such that

$$A_{ij} = \begin{cases} 1 & \text{if there is an edge between nodes } i \text{ and } j, \\ 0 & \text{otherwise.} \end{cases} \quad (2)$$

The natural frequencies  $\{\omega_i\}$  are distributed according to a probability density  $g(\omega)$ , which we will take to be symmetric and centered around a mean frequency of zero.

The overall amount of synchrony in the population at a given time  $t$  is typically quantified with the Kuramoto order parameter [43, 44]

$$R(t)e^{i\psi(t)} = \frac{1}{N} \sum_{j=1}^N e^{i\theta_j(t)}, \quad (3)$$

which can be thought of as the centroid of the  $N$  phases on a unit circle in the complex plane [47]. Here,  $\psi$  is the average phase of the population, and the modulus  $R$ , given by,

$$R(t) = \frac{1}{N} \left| \sum_{j=1}^N e^{i\theta_j(t)} \right|, \quad (4)$$

quantifies the amount of phase coherence. When the oscillators' phases are uniformly spread,  $R \approx 0$  and the system exhibits low synchrony. On the other hand, when the phases become tightly clustered,  $R \approx 1$  and the system exhibits high levels of synchrony.

We can also use this order parameter, which ranges from  $R = 0$  (complete incoherence) to  $R = 1$  (complete phase synchronization), to monitor the global degree of synchrony in the system as a function of the coupling  $\alpha$ . In this case, one typically reports a time-averaged value

$$\langle R \rangle = \frac{1}{T} \int_{T_R}^{T_R+T} R(t) dt \quad (5)$$

computed on an interval of length  $T$  after several transient or relaxation time steps  $T_R$  have been discarded.

## III. MOTIVATION AND THE CO-EVOLUTIONARY MODEL

In this study, we consider a feedback process between dynamics and the restructuring of network topology that integrates different ideas and results from previous studies on adaptation or enhancing synchronization in networks of non-identical Kuramoto oscillators. To better frame and motivate our contributions, we briefly outline some past work on these topics below.

### A. Inspiration from prior investigations

In general, it is expected that different adaptive strategies will lead to the emergence of different patterns in both the network topology and the dynamics, and a number of studies have explored these ideas using, for example, chaotic dynamics [78–80, 99, 100], models of neuronal dynamics [83, 101, 102], and non-identical Kuramoto oscillators [77, 81, 82, 84–89, 103–108]. Focusing on the

latter of these classes, one early study found that dynamical rewiring to force links between nodes with more similar time-averaged frequencies creates strongly synchronized clusters of nodes, and the network reaches a small-world configuration [84]. More recently local, competitive adaptation mechanisms, which tend to strengthen (weaken) connections between more dynamically coherent (incoherent) oscillators have been shown to lead to the emergence of modular organization in Kuramoto networks [77, 88, 89, 105], and positive feedback can simultaneously enhance synchronization and percolation in initially fragmented networks [109]. In complementary efforts, Sendiña Nadal *et al.* [86] and Sendiña-Nadal *et al.* [87] studied a growth process in which heterogeneous oscillators make connections to external pace-maker nodes so as to become locked with the pace-maker dynamics. When the attachment process is preferential and determined from differences in the dynamical states of the heterogeneous oscillators and pace-maker nodes, entrainment occurs simultaneously with the emergence of a power law degree distribution. In addition, adaptive processes that favor the strengthening of edges between more out of phase oscillators, can significantly improve global synchronization in non-identical Kuramoto networks [103, 104]. However, the resulting networks were not necessarily evolved under fixed total weight and the topology was not analyzed in depth for relationships between structure and dynamical properties as a function of the global coupling, both of which are the aims of the present work.

Another line of inquiry has revolved around the problem of optimizing synchronization of non-identical systems of Kuramoto oscillators, in order to understand what structural properties of the network are important. For example, using an optimization procedure to maximize the order parameter  $R$ , Brede [64, 65] uncovered key features that can enhance synchronization. These include the placement of more edges on oscillators with natural frequencies further from the mean (yielding positive correlations between degrees and frequency magnitudes), as well as the preferential attachment of oscillators with large frequencies to other oscillators with smaller frequencies (yielding negative correlations between the intrinsic frequencies of adjacent oscillators). These findings have been corroborated in several other studies on optimizing networks of non-identical Kuramoto oscillators as well [110–113]. Furthermore, forcing positive *versus* negative correlations between adjacent frequencies appears to change the critical coupling and exponents for the synchronization transition [114]. Other work has considered the enhancement of both global and local phase synchronization [115, 116], finding that local synchronization leads to an earlier onset of collective dynamics at lower couplings – facilitated by clustering and the grouping together of nodes with similar frequencies – but makes the state of full synchronization more difficult to achieve. More recently, spectral analyses have been employed to show that synchronization is optimized under

specific couplings of the natural frequencies to eigenvectors of the Laplacian, i.e., when the frequencies are maximally aligned with the largest eigenvector [69–71]. Importantly, the previously reviewed works indeed uncover several crucial network features for optimizing collective dynamics. However, the question of if or via what type of mechanism such networks could be generated or evolved for using solely local adaptive strategies – and how such a process occurs over time and at different couplings – remains open.

In this study, we numerically investigate the interplay between network structure and oscillator dynamics. We report on a local, state-dependent rewiring mechanism that can (i) evolve initially random and uncorrelated networks towards structured configurations with specific relationships between dynamical and topological properties and (ii) through a reciprocal process, simultaneously improve synchronizability. While the ideas of dynamical self-organization from local rules and global network optimization strategies have been studied on separate fronts, here, we attempt to specifically consider them in tandem. In what follows, we first state the initial setup and parameters of the system (Sec. III B) and then describe the co-evolutionary process in detail (Sec. III C).

## B. Initial network construction

All simulations were carried out with a 4<sup>th</sup> order Runge-Kutta method using a time step of  $\Delta t = 0.02$ . Initial phases  $\{\theta_i(0)\}$  were distributed at random in the interval  $[-\pi, \pi]$ , and the natural frequencies  $\{\omega_i\}$  were drawn at random from a uniform distribution in the range  $[-2, 2]$ , denoted as  $\{\omega_U\}$ . In Appendix B), we also show results for the case of a Gaussian distribution with zero mean and unit standard deviation, denoted as  $\{\omega_G\}$ .

The initial network configurations are binary and undirected Erdős-Renyi (ER) random graphs of type  $G(N, L)$  (i.e., the network is drawn from the distribution of random graphs with  $N$  nodes and  $L$  edges), with corresponding average degree  $\langle k \rangle = 2L/N$ . Importantly, this initialization produces networks without special topological characteristics and without relationships between network properties and dynamical properties. We will denote the initial network configurations as  $\mathcal{G}_o$  and the networks at the end of the adaptive process as  $\mathcal{G}_*$ , and similarly we will use ‘o’ and ‘\*’ to denote quantities computed on each network. For the remainder of the main text, we fix  $N = 100$  and examine two different values of  $L$  chosen such that  $\langle k \rangle = 25$  or  $\langle k \rangle = 12.5$ . (In the Supplement [117], we also check the robustness of several results with respect to variations in system size, initial network topology, and frequency distribution). Reported measures correspond to ensemble averages over independent simulations using different instantiations of the initial network, initial phases, and node frequencies.

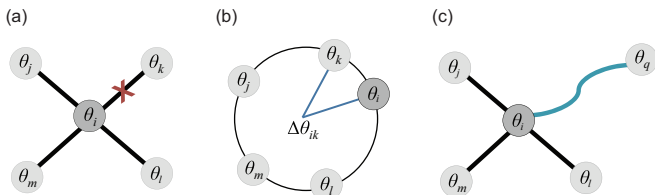


FIG. 1. A schematic of the network update process. (a) At a time  $t_m = T_R + mT$ , node  $i$  is selected at random from all nodes in the network, and it breaks its connection to the node  $k$ , which (b) is the node it is instantaneously most in phase with. (c) A new edge  $(i, q)$  is then created between  $i$  and a randomly selected node  $q$  with phase  $\theta_q$ .

### C. Mechanism of adaptive rewiring

We turn now to an explanation of the co-evolutionary scheme, whereby the network is restructured according to the dynamics. Motivated by previous literature on adaptive Kuramoto networks [103, 104], we take as our starting point a mechanism that aims to suppress the largest instantaneous phase differences between a given node and its nearest neighbors. After setting up the initial conditions and network  $\mathcal{G}_o$  as described in Sec. III B, the dynamics are first run for a long relaxation interval  $T_R$ . Then at regular times  $t_m = T_R + mT$ , where  $m$  is the number of attempted rewirings and  $T$  is an associated period characterizing the adaptation process (which will be some multiple of the time step), rewiring is invoked as follows. A node  $i$  is chosen at random from the network and the quantity

$$f_{ij} = \frac{1}{2}[1 - \cos(\theta_i(t_m) - \theta_j(t_m))] \quad (6)$$

is computed for all  $j \in \mathcal{N}(i)$ , where  $\mathcal{N}(i)$  is the neighborhood of  $i$ . Note that this function is *local* in the sense that it depends only on the instantaneous phases of node  $i$  and of the nodes  $j \in \mathcal{N}(i)$  that are neighbors of  $i$  at the current time  $t_m$ . It takes on a value of 1 when  $\theta_i - \theta_j = \pm\pi$  (maximal phase separation) and a value of 0 when  $\theta_i - \theta_j \bmod 2\pi = 0$  (perfectly in-phase). The edge  $(i, k)$ , where  $k$  is the node in  $\mathcal{N}(i)$  minimizing  $f_{ik}$ , is then broken and a new link  $(i, q)$  is formed between node  $i$  and a randomly selected node  $q$  that is not one of the nodes to which  $i$  maintains a connection. This step corresponds to the breaking and rewiring of the link between node  $i$  and the neighbor  $k$  with which it is currently most in phase (Fig. 1). This set of dynamical update rules are repeated for a large number of switches  $m$ , resulting in an evolved network  $\mathcal{G}_*$ . We use  $m = 2.5 \times 10^4$ , which allows us to observe interesting dynamical and structural changes in the system, while being within enough computational reason to allow for the exploration of several different network and natural frequency parameter changes (however, we also point out places where the capability to run more adaptation steps may offer additional clarity). Finally, once rewiring has ceased, the dynamics continue to run

atop  $\mathcal{G}_*$  for another relaxation interval. For clarity, in the figures that follow, all quantities that change every *time step* will be labeled as “time,  $t$ ”, and all quantities that change only when the network is *rewired* will be labeled as “rewiring step,  $m$ ”.

Before continuing, we wish to point out some features of this mechanism. First, it applies to the case of binary, undirected connectivity, and maintains the density of the network throughout co-evolution. Setting these constraints disambiguates the role of rearrangements in network topology in shaping results from other factors such as increases in the total number of edges, heterogeneous weighting, or directionality. Furthermore, it allows for the cleanest comparison against much of the previous work on optimizing synchronization via rewiring. Second, we note that this adaptive process is a type of repulsive or suppressive strategy, but unlike [78–82, 103, 104], which consider weight plasticity, or [86, 87] which consider a growth mechanism, we consider connectivity reorganization where edges in an initially random configuration are periodically pruned and rewired between the most instantaneously and locally in-phase oscillators, but remain in place between the more locally dissonant oscillators. The random rewiring after edge deletion introduces realistic stochasticity and allows for a sampling of the network, without breaking the locality condition for determining which edge is rewired [75]. Though not a model of a specific system, this type of disassortative mechanism has real-world counterparts. For example, it is in the same vein as anti-Hebbian learning rules in neural systems, where synapses weaken between more dynamically correlated neurons and strengthen between more incoherent neurons [93, 94]. It may also mimic some strategies of opinion formation and influence on social networks, where people preferentially link with those of more different opinions from themselves [118].

## IV. RESULTS

### A. Co-evolved networks exhibit enhanced global synchronization

Our first main result is that the adaptive rewiring mechanism is able to enhance global synchronization over a broad range of coupling values. This result holds for both frequency distributions (See Appendix B for the analysis with the normally distributed frequencies) and values of average degree, and in addition, is robust to an order of magnitude difference in the the structural reconfiguration period,  $T$ .

We first discuss the time evolution of the order parameter  $R(t)$  for the co-evolving networks. Fig. 2 depicts examples of  $R(t)$  vs. time  $t$  for the case of uniformly distributed frequencies  $\{\omega_U\}$  and  $T = 0.2$ . The top row is for  $\langle k \rangle = 25$ , with representative couplings (a)  $\alpha = 0.065$  and (b)  $\alpha = 0.085$ , and the bottom row is for  $\langle k \rangle = 12.5$ , with representative couplings (c)  $\alpha = 0.135$

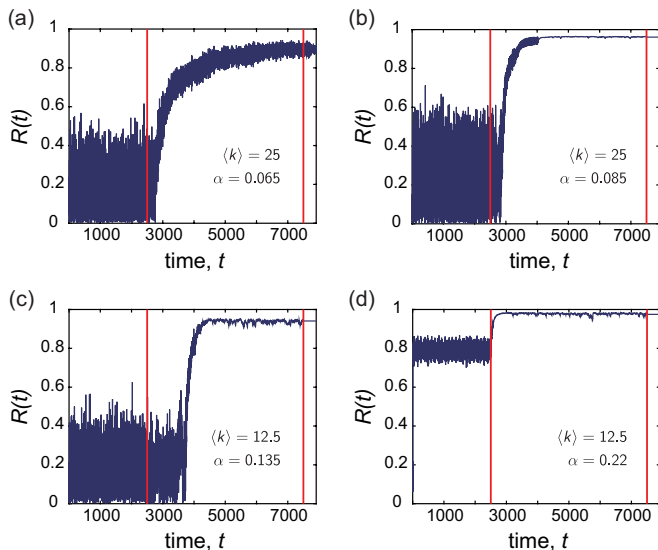


FIG. 2. Examples of the global order parameter  $R(t)$  vs. time  $t$  for various representative couplings  $\alpha$ . In each case, the dynamics were first run atop an initially ER random graph with average degree  $\langle k \rangle$ , after which co-evolution of the network and dynamics took place between the two red lines. The natural frequencies were drawn from the uniform distribution  $\{\omega_U\}$ , and the mean degree  $\langle k \rangle$  and coupling  $\alpha$  used for each panel were (a)  $\langle k \rangle = 25$ ,  $\alpha = 0.065$ , (b)  $\langle k \rangle = 25$ ,  $\alpha = 0.085$ , (c)  $\langle k \rangle = 12.5$ ,  $\alpha = 0.135$ , (d)  $\langle k \rangle = 12.5$ ,  $\alpha = 0.22$ . During the adaptation period, the network was continually rewired once every  $T = 0.2$  time units. The co-evolving networks exhibit enhanced collective dynamics, as observed by increases in the global order parameter.

and (d)  $\alpha = 0.22$ . In each case, the dynamics are first run atop the initially static ER network for several time steps. Adaptation begins at a time denoted by the left red line, and ends after several time steps at the right red line. We observe that at lower coupling values - when the dynamics on the initial network exhibit little coherence across time - the adaptive strategy is able to significantly increase  $R$  to an intermediate value throughout the rewiring stage. However, the order parameter does still exhibit some fluctuations and the system may not reach a perfectly smooth steady-state. As  $\alpha$  is increased, the order parameter in the non-adaptive regime remains fluctuating around an intermediate mean value, but once co-evolution begins, the self-organizing network rearranges such that  $R$  again increases and reaches a value near 1. When rewiring ceases after several cycles, the resulting networks are able to maintain these states of heightened collective dynamics, and the global order parameter stays at the increased value. However, though the time-averaged value  $\langle R \rangle$  remains high for the networks with  $\langle k \rangle = 12.5$ , we find that in some cases the order parameter still exhibits fluctuations, even after the adaptation period has ceased. This intuitively suggests that the co-evolved networks with higher average degree are more robust to the stochasticity in the rewiring and

the exact placement of edges in the network, in terms of their ability to support a frequency synchronized state. Sec. B 1 contains additional figures of  $R(t)$  vs. time for the case of normally distributed frequencies.

In order to obtain a more complete picture of the effect of adaptive rewiring, we performed a sweep over a comprehensive coupling range. For  $\langle k \rangle = 12.5$  we considered a range  $\alpha \in [0, 0.4]$ , and for  $\langle k \rangle = 25$ , we considered  $\alpha \in [0, 0.2]$ ; in both cases, couplings were sampled at a resolution  $\Delta\alpha = 0.005$ . At each value of  $\alpha$ , networks and initial conditions were initialized as described in Sec. III B. We then ran a set of simulations on the original, uncorrelated networks  $\mathcal{G}_o$ , and obtained a time-averaged value of the global order parameter  $\langle R \rangle$  (Eq. 5) over the last  $1 \times 10^4$  time steps. A second set of simulations were then run with the same initial conditions, but under the co-evolutionary scheme (i.e. the network topology was allowed to co-evolve with the dynamics for  $m$  rewiring steps, after which a time-averaged order parameter was computed on the final adapted network  $\mathcal{G}_*$ ).

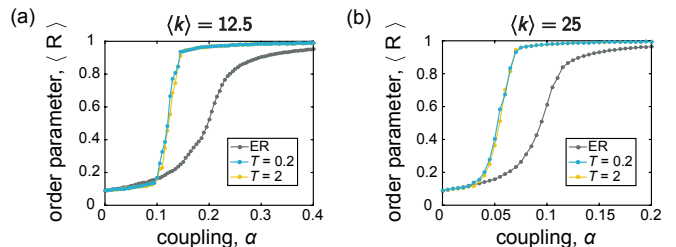


FIG. 3. The time-averaged order parameter vs. coupling. In each panel, the gray data points correspond to static ER random graphs  $\mathcal{G}_o$ , and the blue and yellow points correspond to the adapted networks  $\mathcal{G}_*$  evolved under rewiring time scales of  $T = 0.2$  and  $T = 2$ , respectively. The frequencies were drawn from the uniform distribution  $\{\omega_U\}$ , and the mean degree of the networks are (a)  $\langle k \rangle = 12.5$ , and (b)  $\langle k \rangle = 25$ . All curves depict averages over 25 instantiations, and the lines between data points serve as guides for the eye.

We show the outcome of this analysis in Fig. 3, where each panel is a plot of  $\langle R \rangle$  vs.  $\alpha$ . Panels (a) and (b) correspond to networks with  $\langle k \rangle = 12.5$  and  $\langle k \rangle = 25$ , respectively. Furthermore, we plot curves for two different values of the waiting time between structural changes to the network:  $T = 0.2$  and  $T = 2$ . As can be seen from each of the curves, there is a broad range of  $\alpha$  over which the regulatory mechanism for network restructuring leads to improvements (higher values) of the time-averaged global order parameter. This enhancement does not begin immediately at  $\alpha = 0$ , but once the coupling is high enough (still at a relatively low value), the order parameter begins to increase at a much steeper rate, and  $\langle R \rangle$  remains noticeably higher for the adaptive networks  $\mathcal{G}_*$  versus the static networks  $\mathcal{G}_o$ , across all couplings beyond a certain point. These trends are robust for both rewiring periods and average degrees, and as can be seen in Sec. B 1, the results hold for the case of normally distributed natural frequencies. (The Supplementary Material [117] shows

additional and qualitatively similar findings for simulations on slightly larger networks or those with lower mean degree, and for the case of a non-symmetric frequency distribution). It is also worth noting that – although the total number of times the network is allowed to rewire is limited by computational constraints – since there is no built-in condition for adaptation to cease and since there is a stochastic component to the network reconfiguration, the ability to run more adaptation steps may yield even further improved results.

### B. Emerging structure and correlations between network topology and dynamical properties

Given that dynamical reconfiguration of the network - informed by local information on the states of connected oscillators - can improve the overall amount of synchronization in the system, a second line of inquiry is understanding what properties of the evolved networks lend themselves to this capability. In particular, does the self-enacted rewiring mechanism generate the interesting topological features and correlations that arise with global optimization schemes, which in a cyclic process, then allow synchronization to occur?

We begin by investigating the networks  $\mathcal{G}_\star$  for certain relationships between their topology and the natural frequencies of the oscillators. Two properties in particular – degree-frequency correlations and frequency-neighbor frequency correlations – have been associated with networks optimized for synchronization [64, 65, 69] as well as with the phenomenon of explosive synchronization [66, 67] (see Sec. I and Sec. III).

Though the natural frequencies of each node remain fixed here, the way oscillators of different frequencies are coupled to one another changes over time from the initial, random configuration to the end of adaptation. In Fig. 4, we show examples of how two specific relationships manifest in an ER network  $\mathcal{G}_o$  and the corresponding adaptively rewired network  $\mathcal{G}_\star$ . The top and bottom two rows of Fig. 4 are for networks with  $\langle k \rangle = 12.5$  and  $\langle k \rangle = 25$ , respectively, and in both cases, the first column corresponds to the ER network and the second column corresponds to the rewired network. For each node  $i$ , we first computed its offset (or difference) from the mean frequency  $\tilde{\omega}_i = \omega_i - \langle \omega \rangle$ , where  $\langle \omega \rangle$  is the mean intrinsic frequency of the population. Panels (a,b) and (g,h) then show node degree  $k_i$  vs. frequency offset  $\tilde{\omega}_i$ , and panels (d,e) and (j,k) show the average frequency offset of oscillator  $i$ 's neighbors  $\langle \tilde{\omega}_j \rangle$  ( $\forall j \in \mathcal{N}(i)$ ) vs. frequency offset  $\tilde{\omega}_i$ . Note that the coupling values  $\alpha$  are such that the original networks exhibited intermediate synchrony, but the self-organized networks were able to entrain the population to a high level of synchrony.

As expected, initially there is little correlation present between topological properties and the dynamical property of oscillator frequency, as illustrated by the lack of organization in the plots in the first column of Fig. 4.

However, from observation of the second column, it is evident that when the co-evolutionary update scheme can enhance synchronization, it simultaneously leads to the emergence of very specific correlations between network topology and oscillator frequencies. We first note the appearance of the marked v-shaped curves characterizing the plots of  $k_i$  vs.  $\tilde{\omega}_i$  (panels (b) and (h)), which signify that the node degrees become positively correlated with the absolute value of the oscillator frequency offsets. In other words, nodes with natural frequencies further from the mean frequency of the population gather proportionately more edges.

A second finding is that when increased global synchrony arises from a restructuring of the network, the final arrangement exhibits distinct relationships between the frequency of a given oscillator and the frequencies of that oscillators' direct neighbors on the network. The patterns in panel (e) and (k) showing  $\langle \tilde{\omega}_j \rangle$  vs.  $\tilde{\omega}_i$  points to the fact that each oscillator tends to be connected to other oscillators with, on average, natural frequencies on the opposite side of the mean frequency. Since the mean frequency  $\langle \omega \rangle \approx 0$  for the distributions we consider, this implies that oscillators with positive frequencies become surrounded by oscillators with negative intrinsic frequencies, and vice-versa. In Sec. A we also define an additional measure of this organization as the correlation  $C_{\tilde{\omega}, \sum \tilde{\omega}}$  between the magnitude of the natural frequency offsets and the sum of the magnitude of neighbor frequency offsets. Fig. 11 shows examples of this quantity for the same networks as those in Fig. 4.

To quantify these relationships and study how they evolve with the number of rewiring steps, we considered two summary statistics, following [64, 65, 114, 115]. The first of these measures is a simple (Pearson) correlation coefficient,  $C_{|\tilde{\omega}|,k}$ , to quantify the strength of the relationship between degree and frequency magnitude offset. This measure increases steadily as throughout co-evolution of the network and dynamics (Fig. 4c,i). In addition, for each node  $i$  we calculated the fraction of its neighbors  $f_i$  with natural frequencies on the opposite side of the mean, as compared to node  $i$ 's frequency, and then computed an average  $f$  over all  $f_i$  (i.e over all nodes in the network). This metric also increases as the network is rewired, as observed in Fig. 4f,l. Also see Fig. 11 for an example of the evolution of the additional measure,  $C_{\tilde{\omega}, \sum \tilde{\omega}}$ .

We have thus far shown examples of emerging structural patterns that arise for the situation when the evolving network is clearly able to entrain the nodes to a state of higher synchrony. However, the ability of this behavior to occur is also dependent on the coupling  $\alpha$ . In order to better understand the appearance of topological and dynamical correlations and their dependence on the overall coupling, we computed the same measures ( $C_{|\tilde{\omega}|,k}$  and  $f$ ) as a function of  $\alpha$  (see Figs. 5,6, respectively). In each case, the measures were computed on the final networks  $\mathcal{G}_\star$  at the end of adaptation.

For each combination of natural frequency distribu-

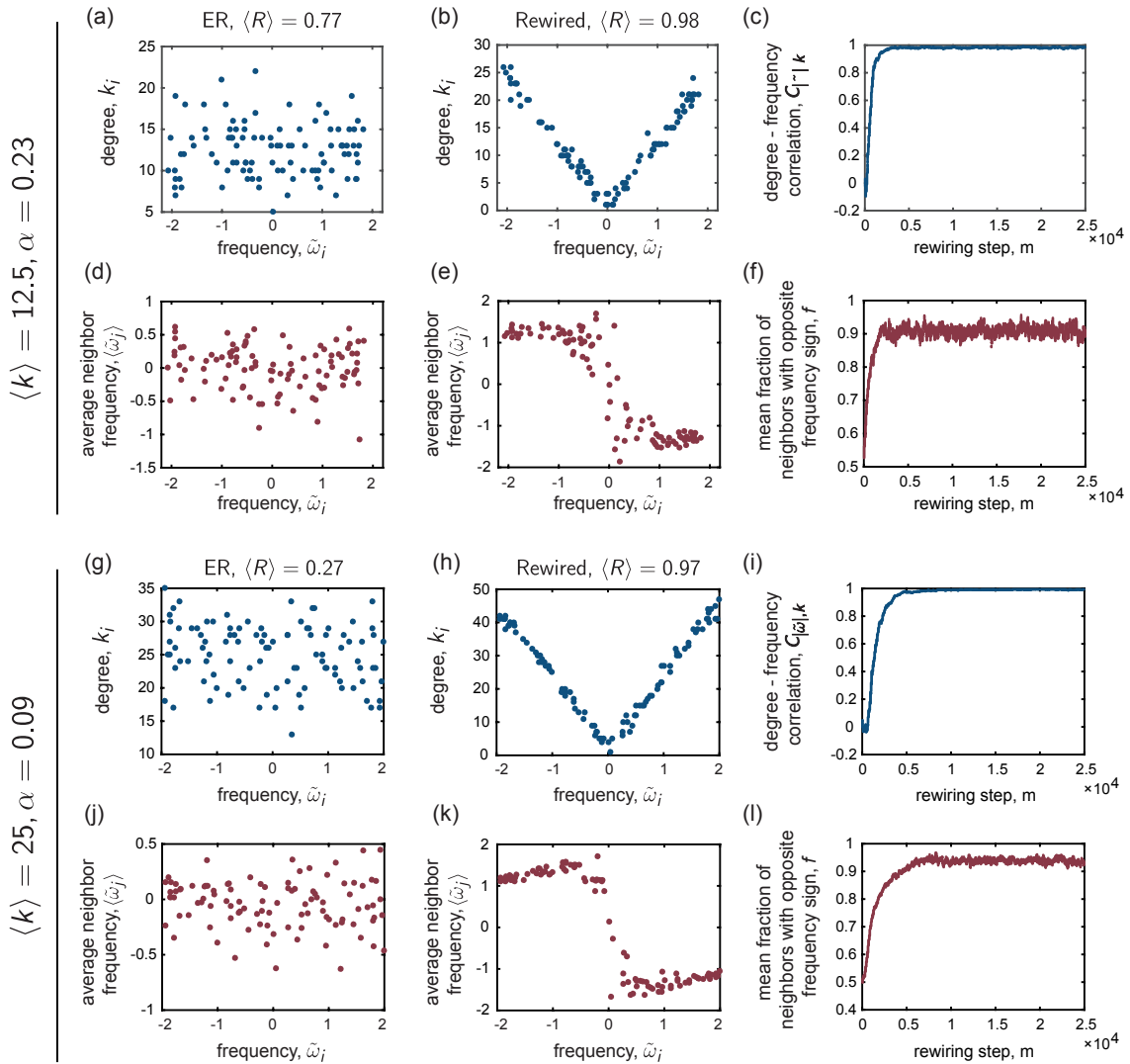


FIG. 4. Relationships between the network structure and the intrinsic frequencies of the oscillators. The top two rows show examples for a network with  $\langle k \rangle = 12.5$ , and the bottom two rows show examples for a network with  $\langle k \rangle = 25$ ; in both cases, the frequencies were drawn from the uniform distribution  $\{\omega_U\}$ . For each network density, the first column corresponds to an ER random graph that exhibits only intermediate levels of synchrony (as measured by  $\langle R \rangle$ ) at the displayed coupling  $\alpha$ , and the second column corresponds to the adapted network, which exhibits a higher level of synchrony. These plots highlight key relationships that emerge from the co-evolutionary network update rule. (a,b); (g,h) Node degree  $k_i$  vs. frequency offset  $\tilde{\omega}_i$ . (d,e); (j,k) Average neighbor frequency offset  $\langle \tilde{\omega}_j \rangle$  vs. frequency offset  $\tilde{\omega}_i$ . (c); (i) The correlation  $C_{|\tilde{\omega}_i|, k}$  between node degree  $k_i$  and the magnitude of the frequency offset  $\tilde{\omega}_i$  vs. the number of rewiring steps  $m$ , and (f); (l) the fraction  $f$  of an oscillator's neighbors that have frequency offsets of opposite sign compared to the given oscillator (averaged over all nodes in the network) vs. the number of rewiring steps  $m$ .

tion, average degree, and rewiring period, we observe robust trends. In particular,  $C_{|\tilde{\omega}_i|, k}$  remains near zero at low coupling values, and then proceeds to quickly increase as a function of  $\alpha$  until it saturates to a nearly steady value (close to 1). In other words, as the overall coupling increases, the degree-frequency magnitude correlation becomes more apparent. The frequency-neighbor frequency relationships follows a similar evolution. Specifically, the mean fraction of an oscillator's neighbors with frequencies on the opposite side of the mean also grows with  $\alpha$ , plateauing near a high value of  $f \approx 0.9$ . This points to

a heightened mixing of oscillator types that arises with increased coupling. We also refer the reader to Fig. 12 for the analysis of the supplementary quantity,  $C_{\tilde{\omega}, \sum \tilde{\omega}}$ , which supports and further aids in the understanding of these findings.

There are three main features in these trends worth pointing out explicitly. First, for the network rewiring periods considered here, the general form of the curves appears to be independent of the time  $T$  between a structural perturbation to the network. Second, the two quantities considered,  $C_{|\tilde{\omega}_i|, k}$  and  $f$ , both exhibit a clear

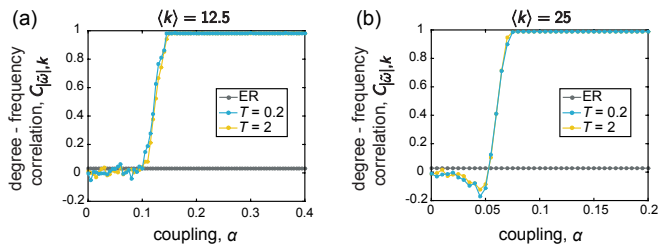


FIG. 5. These plots depict the correlation  $C_{|\tilde{\omega}|,k}$  between node degree  $k_i$  and the magnitude of the frequency offset  $|\tilde{\omega}_i|$ , as a function of the coupling. In each panel, the blue data points correspond to the initial, uncorrelated ER random graphs  $\mathcal{G}_o$ , and the orange and yellow points correspond to the adapted networks  $G_*$  evolved under rewiring time scales of  $T = 0.2$  and  $T = 2$ , respectively. The frequencies were drawn from the uniform distribution  $\{\omega_U\}$ , and the mean degree of the networks are (a)  $\langle k \rangle = 12.5$ , and (b)  $\langle k \rangle = 25$ . The dip observed in (b) at  $\alpha \approx 0.5$  is due to the localization of edges on a cluster of oscillators with natural frequencies near the mean; this is examined further in Sec. IV C. All curves depict averages over 25 instantiations, and the lines between data points serve as guides for the eye.

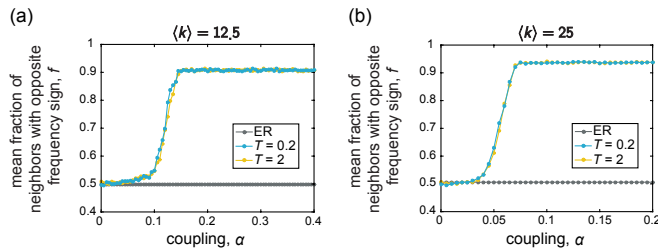


FIG. 6. These plots depict the mean fraction  $f$  of an oscillator's neighbors that have natural frequency offsets of opposite sign compared to that of the given oscillator, as a function of the coupling. In each panel, the blue data points correspond to the initial, uncorrelated ER random graphs  $\mathcal{G}_o$ , and the orange and yellow points correspond to the adapted networks  $G_*$  evolved under rewiring time scales of  $T = 0.2$  and  $T = 2$ , respectively. The frequencies were drawn from the uniform distribution  $\{\omega_U\}$ , and the mean degree of the networks are (a)  $\langle k \rangle = 12.5$ , and (b)  $\langle k \rangle = 25$ . All curves depict averages over 25 instantiations, and the lines between data points serve as guides for the eye.

change in behavior (in terms of the onset of either a rapid increase or decrease) at approximately the same coupling. Thus, in the proposed co-evolutionary scheme, the emergence of these correlations and relationships between topology and properties of the dynamics seem to arise in tandem to one another, in that the appearance of one feature appears to imply the development of the other. A final important observation is that the coupling at which these patterns begin to take shape is near the coupling at which the global order parameter begins to rise (compare to Fig. 3). (Fig. 12 shows that consistent behavior is found for  $C_{\tilde{\omega}, \sum \tilde{\omega}}$  as well). Thus, as found by Brede [64, 65, 114, 115] in his work on optimization

of synchronization of non-identical oscillators, enhanced collective behavior co-occurs with the materialization of specific dynamical and topological relationships. Here, we have shown that organized structure in the form of these correlations can emerge in the network from a simple, adaptive mechanism based on a combination of local state information and stochastic rewiring. We also again note that, although computationally expensive, allowing the co-evolution to run longer may give heightened results, especially at low to intermediate couplings.

### C. Analysis of the time-dependence of the adaptive mechanism

Our analysis thus far has considered the global order parameter and the correlations between the intrinsic frequencies and the network topology that arise in the adaptively rewired networks, and we have mainly focused on a long-time limit of these properties and how they depend on the overall coupling. While Figs. 2 and 4 do briefly examine the time-dependence of these properties as well, in order to gain a further understanding of the adaptation mechanism, we carry out a more in-depth exploration of how the co-evolutionary process unfolds over time at different couplings, and also how individual oscillators with different intrinsic dynamical properties (i.e. intrinsic frequencies) are affected by the rewiring mechanism.

#### 1. Evolution of the instantaneous frequencies

To investigate the temporal evolution of the system - and how the adaptive scheme works from a more local standpoint - we first examine the evolution of the instantaneous frequencies  $\theta_i(t)$  as a function of time. Recall that the condition for a frequency-synchronized state corresponds to the instantaneous frequencies of all oscillators locking to the mean natural frequency of the population,  $\langle \omega \rangle$ . Thus, to better understand the mechanism of the co-evolution process, we specifically consider how oscillators of different *intrinsic* frequencies (in terms of how close or far  $\omega_i$  is to the average natural frequency  $\langle \omega \rangle$ ) evolve as a function of time, and how they may be differentially affected by the time-dependent rewiring of the network. Fig. 7 shows examples of  $\theta_i(t)$  vs.  $t$  for several values of the coupling  $\alpha$  around the point in which the dynamics transition to a synchronized state. The top set of panels (a) are for a network with  $\langle k \rangle = 12.5$ , and the bottom set of panels (b) are for a network with  $\langle k \rangle = 25$ ; in both cases the frequencies are uniformly distributed (Appendix B 3 contains additional figures and discussion for examples with normally distributed frequencies). Each row corresponds to one oscillator, and the rows are ordered by the quantity  $\tilde{\omega}_i = \omega_i - \langle \omega \rangle$  (i.e. the offset from the mean). Adaptation of the network sets in at the time denoted by the black line.

At very low coupling, adaptively rewiring the network

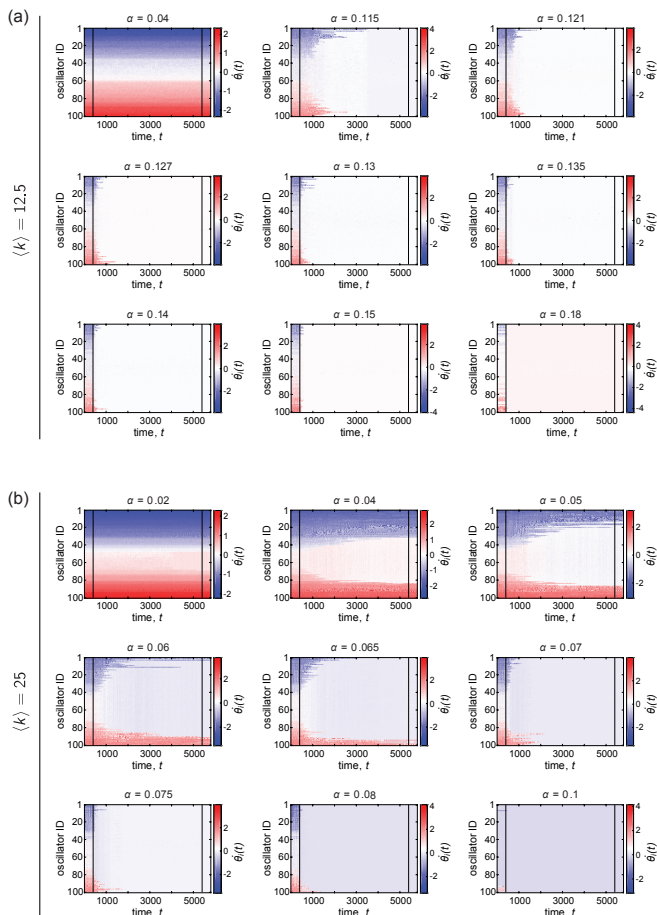


FIG. 7. Examples of the instantaneous frequencies  $\hat{\theta}_i(t)$  vs. time  $t$ , for various representative couplings  $\alpha$ . The mean degree of the networks are (a)  $\langle k \rangle = 12.5$  and (b)  $\langle k \rangle = 25$ , and the natural frequencies  $\{\omega_U\}$  were drawn from the uniform distribution. In all panels, each row corresponds to one oscillator, and the rows are ordered by the quantity  $\tilde{\omega}_i = \omega_i - \langle \omega \rangle$  (i.e. the offset from the mean intrinsic frequency of the population). For each coupling, the dynamics were first run atop an initially ER random graph, after which co-evolution of the network and dynamics took place between the two black lines. During the adaptation period, the network was continually rewired once every  $T = 0.2$  time units.

appears to have negligible effect on the instantaneous frequencies. As the coupling increases to an intermediate value near the transition to synchronization (see Fig. 3), we observe a change in the dynamics; oscillators with intrinsic frequencies near the center of the distribution start evolving with a frequency near the mean earliest, and then later in time, more outlying oscillators become incorporated into the synchronized group. For the denser networks in particular, there are a few sampled coupling values for which the co-evolution results in partial synchronization of those oscillators around the center of the natural frequency distribution, but the synchronized core does not extend to the most disparate oscillators. Thus, there does seem to be a dependence on the natural fre-

quencies in terms of how the co-evolution develops over time. However, at even larger coupling, the transition in the dynamics becomes much faster, and the dependence on the intrinsic frequencies is less noticeable.

Before continuing, we note that the figures shown here (and throughout the rest of Sec. IV C) are for single realizations of the initial network topology and the intrinsic frequencies. For these particular instantiations, we have attempted to sample coupling values that highlight different regimes - in regards to the behavior over time and the overall outcome - of the adaptive rewiring. However, it is important to state that over different realizations, we observe variability in terms of whether or not the rewiring is able to cause significant changes in the dynamics and the network structure at a given coupling; this is especially apparent for the sparser networks and low values of  $\alpha$ . Though it is beyond the scope of the current work, it may be interesting in future work to investigate the degree of this variability and its dependence on the frequency distribution and properties of the network such as density.

## 2. Evolution of the correlations between topology and natural frequencies

We know from Sec. IV B that increases in the order parameter due to the adaptive mechanism are accompanied by the emergence of correlations between the network topology and the oscillator frequencies. Therefore, we now further examine how the network organization restructures over time as the system co-evolves. We focus in particular on the evolution of the degree of individual oscillators across time, and also consider how the degree-natural frequency relationship proceeds due to network rewiring at different values of the global coupling.

Fig. 8 shows the node degree  $k_i$  vs. the rewiring step  $m$  and Fig 9 shows the degree - frequency correlation  $C_{|\tilde{\omega}|,k}$  vs. the rewiring step  $m$  for the same set of networks, natural frequencies, and coupling values as those in Fig. 7. Since we observe some interesting differences for  $\langle k \rangle = 12.5$  (panel (a)) vs.  $\langle k \rangle = 25$  (panel (b)), we discuss each in turn.

For  $\langle k \rangle = 12.5$  and at low coupling, the rewiring does not noticeably affect how edges are distributed on particular oscillators, and  $C_{|\tilde{\omega}|,k}$  fluctuates around zero. As the coupling increases, however, the co-evolution begins to cause significant changes in the network. In particular, there is a short period of time in which edges become concentrated on oscillators with natural frequencies near the mean, whereas oscillators with intrinsic frequencies on the ends of the distribution remain with relatively low degrees. This is then followed by the gradual spreading out of edges onto the more outlying oscillators. We can quantify this behavior by considering the value of the correlation  $C_{|\tilde{\omega}|,k}$  between the absolute value of the frequency offset  $|\tilde{\omega}_i|$  and the node degree  $k_i$ . At  $\alpha = 0.115$ , we see that a slight *negative* degree-frequency correlation

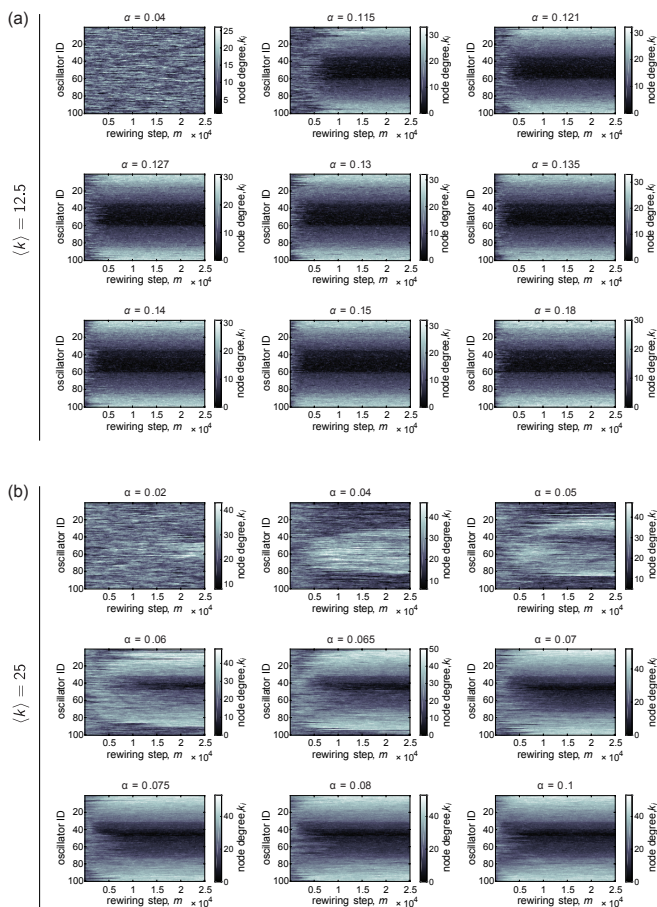


FIG. 8. Examples of the evolution of the node degree  $k_i$  vs. the rewiring step  $m$ , for various representative couplings  $\alpha$ . The mean degree of the networks are (a)  $\langle k \rangle = 12.5$  and (b)  $\langle k \rangle = 25$ , and the natural frequencies  $\{\omega_U\}$  were drawn from the uniform distribution. In all panels, each row corresponds to one oscillator, and the rows are ordered by the quantity  $\tilde{\omega}_i = \omega_i - \langle \omega \rangle$  (i.e. the offset from the mean intrinsic frequency of the population). The network was continually rewired once every  $T = 0.2$  time units.

develops briefly in the initial stages of the rewiring, followed by an increase to a high, positive value. As the coupling increases further, the period of negative degree-frequency correlation disappears, and the edges rapidly redistribute onto oscillators with the most disparate intrinsic frequencies.

Interestingly, we observe slightly different behavior in terms of how network adaptation unfolds for the case of  $\langle k \rangle = 25$ . In particular, at low coupling values, there is regime during which edges consistently build up on oscillators with natural frequencies near the center of the distribution. This results in  $C_{|\tilde{\omega}|,k}$  becoming significantly negative due to the co-evolution of the network and dynamics, and unlike the situation in the sparser networks, this behavior can persist across the entire rewiring period (see, for example,  $\alpha = 0.05$ ). The concentration of edges on oscillators near the center of the distribution

explains the dips in Fig. 5b, which shows  $C_{|\tilde{\omega}|,k}$  vs.  $\alpha$  for the case of  $\langle k \rangle = 25$ . We also note that near the value of the coupling where the dip occurs, the order parameter for the rewired networks begins to deviate from that of the ER networks (Fig. 3b), likely due to the formation of a locally synchronized cluster. This organization does not seem to occur for the sparser networks, suggesting an interesting dependence on the network density; this may be an interesting parameter to explore further in future work. For slightly larger couplings, we observe a change in behavior in terms of how the adaptive mechanism affects the network. In particular - as a function of rewiring step - we observe that at intermediate values of  $\alpha$  there is first an increase in degree for oscillators with frequencies more closely surrounding the mean, which gives rise to a slightly negative degree-frequency correlation. But, as the network continues to co-evolve, edges begin to move towards more outlying oscillators, and the degree-frequency correlation crosses zero and then starts to become positive. However, the most disparate oscillators may still not be able to gather enough edges, resulting in a positive correlation that is less than 1 (i.e., there is some scatter in the relationship). At even higher couplings,  $C_{|\tilde{\omega}|,k}$  almost immediately begins to rise, rather than decreasing first. In addition, the correlation quickly saturates at a value close to 1, signifying a very strong degree-frequency relationship that extends to even the oscillators on the far edges of the natural frequency distribution. Thus, at large couplings the time evolution of the adaptive mechanism is similar for  $\langle k \rangle = 12.5$  and  $\langle k \rangle = 25$ . If network co-evolution were allowed to increase for an even longer time, we may observe a plateauing in  $C_{|\tilde{\omega}|,k}$  for intermediate values of  $\alpha$ , though likely not at a level corresponding to a near-perfect positive relationship.

#### D. Spectral Analysis

As an additional connection to recent literature on optimizing synchronization in heterogeneous oscillator populations, we also carry out a spectral analysis, following the work of Skardal *et al.* [69]. In a series of papers [69–71], the authors derived conditions describing the deviation from full phase locking, and also uncovered conditions for promoting synchronous dynamics. By considering a linearized form of the equations of motion valid in the high-synchrony regime, one of the main analytical results is that the global order parameter,  $R$  can in general be optimized by aligning the vector of intrinsic frequencies  $\tilde{\omega}$  with the dominant eigenvector  $\mathbf{v}_N$  of the Laplacian matrix  $\mathbf{L}$  (where the elements of the Laplacian are defined as  $L_{ij} = \delta_{ij}k_i - A_{ij}$ ). Given the enhanced synchronization found here, it is interesting to ask whether the local rewiring rule that we study generates networks with similar spectral properties.

To address this question, we examine the quantity  $|\langle \frac{\tilde{\omega}}{\|\tilde{\omega}\|}, \frac{\mathbf{v}_N}{\|\mathbf{v}_N\|} \rangle|$ , where  $\frac{\tilde{\omega}}{\|\tilde{\omega}\|}$  is the (normalized) vector of

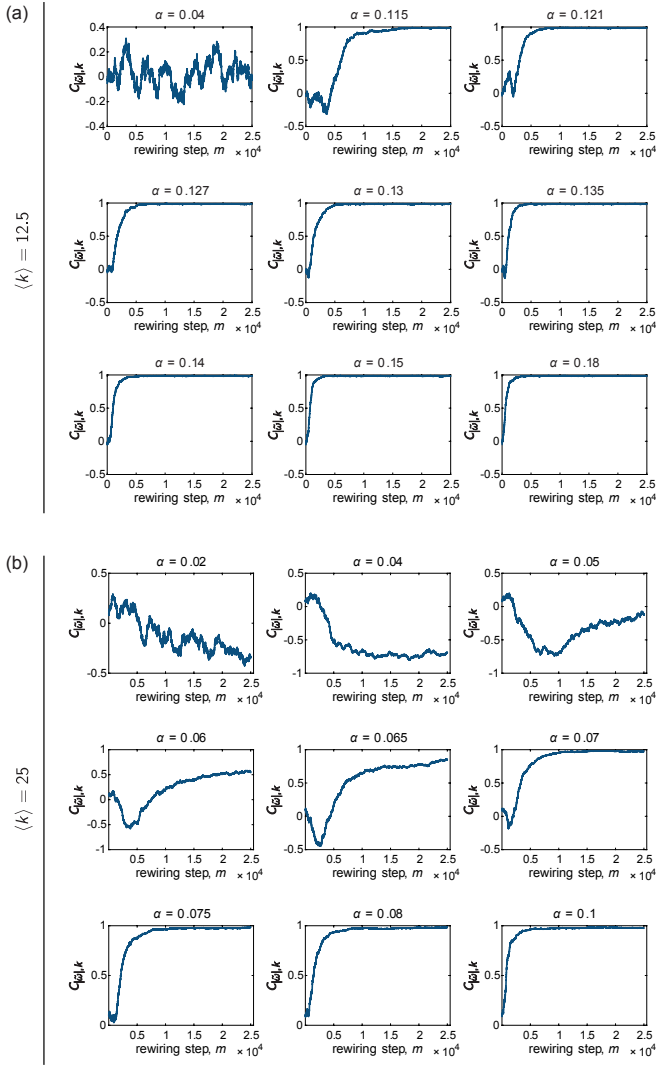


FIG. 9. Examples of the evolution of the correlation  $C_{|\tilde{\omega}|,k}$  between oscillator frequency offset  $\tilde{\omega}_i$  and the node degree  $k_i$ , vs. the rewiring step  $m$ , for various representative couplings  $\alpha$ . The mean degree of the networks are (a)  $\langle k \rangle = 12.5$  and (b)  $\langle k \rangle = 25$ , and the natural frequencies  $\{\omega_U\}$  were drawn from the uniform distribution. In all panels, each row corresponds to one oscillator, and the rows are ordered by the quantity  $\tilde{\omega}_i = \omega_i - \langle \omega \rangle$  (i.e. the offset from the mean intrinsic frequency of the population). The network was continually rewired once every  $T = 0.2$  time units.

natural frequency offsets, and  $\frac{\mathbf{v}_N}{\|\mathbf{v}_N\|}$  is the (normalized) dominant Laplacian eigenvector. In order to understand the dependence of this frequency-eigenvector alignment on the coupling strength, at each value of  $\alpha$  we compute  $|\langle \frac{\tilde{\omega}}{\|\tilde{\omega}\|}, \frac{\mathbf{v}_N}{\|\mathbf{v}_N\|} \rangle|$  on the final, co-evolved networks  $\mathcal{G}_*$ , as well as on the original ER networks  $\mathcal{G}_o$  for comparison. Fig. 10 (a) and (b) show this analysis for the two different values of the mean degree (see Fig. 22 for the corresponding analysis with normally distributed frequencies). At low coupling,  $|\langle \frac{\tilde{\omega}}{\|\tilde{\omega}\|}, \frac{\mathbf{v}_N}{\|\mathbf{v}_N\|} \rangle|$  for the rewired networks remains low, near its initial value. Note that in

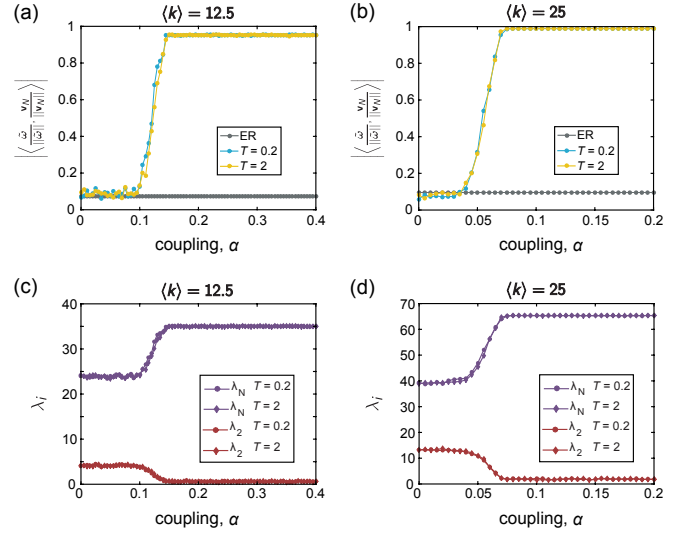


FIG. 10. A spectral analysis of the adaptively rewired networks. (a, b) Evolution of the overlap  $|\langle \frac{\tilde{\omega}}{\|\tilde{\omega}\|}, \frac{\mathbf{v}_N}{\|\mathbf{v}_N\|} \rangle|$  between the intrinsic frequencies  $\tilde{\omega}$  and dominant Laplacian eigenvector  $\mathbf{v}_N$  as a function of the coupling. In each panel, the gray data points correspond to the original, uncorrelated ER random graphs  $\mathcal{G}_o$ , and the blue and yellow curves correspond to the adapted networks  $\mathcal{G}_*$  evolved under rewiring time scales of  $T = 0.2$  and  $T = 2$ , respectively. (c, d) Evolution of the first non-zero eigenvalue  $\lambda_2$  (maroon data) and the largest eigenvalue  $\lambda_N$  (purple data) of the Laplacian  $\mathbf{L}$  as a function of the coupling. In each panel, the eigenvalues were computed on the final adapted networks  $\mathcal{G}_*$  evolved under rewiring time scales of  $T = 0.2$  (circles) and  $T = 2$  (diamonds). The natural frequencies were drawn from the uniform distribution  $\{\omega_U\}$ , and the mean degree  $\langle k \rangle$  of the networks are (a, c)  $\langle k \rangle = 12.5$ ; (b, d)  $\langle k \rangle = 25$ . All curves depict averages over 25 instantiations, and the lines between data points serve as guides for the eye.

this regime the order parameter is low as well (Fig. 3). As  $\alpha$  increases, however, the frequency-eigenvector overlap begins to grow, and rapidly increases until a leveling with further increase in the coupling; the plateau occurs close to the maximal value of one for both values of the mean degree. As with the relationships between natural frequency and node degree and natural frequency and neighbor frequencies considered in the previous section, the increasing projection of the intrinsic frequencies onto the dominant Laplacian eigenvector is accompanied by an increase in  $R$ . Thus, the adaptive reconfiguration can cause persistent changes to the organization of the network that are consistent with the conditions predicted by Skardal *et al.* [69] for optimizing synchronization, and the result becomes more prominent at higher coupling. The investigation for the case of normally-distributed frequencies yields similar conclusions (see Appendix B 4, Fig. 22). This analysis provides a more analytical understanding of how the adaptive process is able to enhance the synchronization in the system.

In addition, we examined the behavior of the first non-

zero eigenvalue  $\lambda_2$  and the largest eigenvalue  $\lambda_N$  as a function of the coupling. When analyzing networks of identical oscillators, the ratio  $\lambda_N/\lambda_2$  is often used as a measure of the stability of the synchronized state, with lower values of the ratio corresponding to better synchronizability of the network [62, 63]. Fig. 10(c) and (d) show these quantities for the two different values of the mean degree (see Fig. 22 for the corresponding analysis with normally distributed frequencies). We observe that  $\lambda_N$  for the rewired networks tends to increase from its original value as the coupling increases, while  $\lambda_2$  tends to decrease. Thus, the higher the coupling, the more the co-evolution can increase the eigenvalue gap (i.e. the larger the eigenratio becomes). Interestingly, these trends are in contrast to the optimal conditions for synchronizing identical oscillators, highlighting the fact that the individual dynamical properties of each node play an important role in the adaptive scheme and in turn, the re-organization of the network that allows for enhanced collective dynamics. The results of this spectral analysis for the case of natural frequencies drawn from the normal distribution are consistent with those described here (see Appendix B 4, Fig. 22).

## V. DISCUSSION AND CONCLUSIONS

In this study, we examined co-evolution of network topology and Kuramoto phase-oscillator dynamics as a means to evolve initially unstructured networks towards organized architectures, and to simultaneously enhance synchronization in the system. In terms of the interplay between network topology and synchronization, it has been found that the presence of specific correlations between the structural layout of the network and the dynamical property of oscillator frequencies can greatly augment global synchronization. But these relationships usually arise through optimization strategies that utilize global information about the network or of node properties and states as a function of time [64, 65, 69–71, 110–116]. On the other hand, a different set of work has shown that adaptive strategies that suppress phase differences between Kuramoto oscillators [103, 104] can lead to heightened synchronization. But in the latter case, the interactions between the topology of the adaptive networks and the node frequencies has not been explored or examined in depth. An interesting line of investigation is to therefore understand whether an adaptive rule for updating the structure of the network – based on local dynamical information – can shape the topological patterns and correlations with dynamical properties, whose emergence simultaneously enhances synchronization. To this end, we studied a type of disassortative mechanism in which the edge between a randomly selected node and its most instantaneously synchronized neighbor is stochastically rewired, while all other edges are maintained. Co-evolution of the dynamics and network connectivity occurs through the repetition of this

feedback process, whereby an initially random network continually reconfigures in response to the states of locally connected oscillators.

Through numerical simulation, we examined the time-evolution of this process and the dependence on the global coupling. We found that for a significant coupling range, the rewiring strategy was able to bring the system to a state of heightened collective behavior, as measured by the global order parameter. It is interesting to note that this eventual state of heightened global coherency depended on the adaptive prevention of local synchronization, suggesting a trade-off between local and global dynamics. Other work on adaptive Kuramoto networks has shown that the opposite type of rule, i.e. a competitive strategy which strengthens connections between more in-phase oscillators at the expense of weakening connections elsewhere, leads to modular organization and hence enhanced local rather than global synchrony [88, 89, 105]. Perhaps most importantly, the enhancement of synchronization indeed co-occurred with the emergence of several of the key topological and dynamical correlations shown to arise through optimization of the global order parameter. In particular, when the oscillators exhibited more coherent dynamics, the evolved networks tended to exhibit (1) positive correlations between node degree and magnitude of oscillators’ difference in natural frequency from the mean of the population, and (2) the preference of connections between oscillators with frequency offsets on opposite sides of the mean frequency. We found that the emergence of these relationships and how the adaptive scheme reorganized the network topology over time depended on the global coupling parameter, as well as the intrinsic frequencies and density of the network. We note that in addition to enhancing synchronization [64, 65, 114, 115], the purposeful placement of these types of correlations has also been associated with first order, or explosive, synchronization transitions [66–68]. Far fewer studies, however, have considered how these structural patterns and relationships might arise in a network from local rearrangements or adaptation (though see [107] for one example).

It is important to state that the results found in this study are in line with previous work that has examined adaptive schemes in which weights grow or shrink as a function of phase differences, which also find that rules that actively suppress differences in state are able to improve synchronization. However, there are some important distinctions between the strategies studied in [103] and the one studied here. In regards to the former, the network starts as completely disconnected, with no edges between any oscillators. The edge weights between *all* pairs of nodes are then allowed to increase, up to some bound. In this way, the total density of the network is allowed to change, connections can theoretically occur between all pairs of oscillators at a given time, and the individual edge weights can fluctuate. Other work has considered a situation in which the *topology* of the network is pre-defined and constant, while the weights

can change [104]. On the other hand, we wished to consider a situation in which the effect of topological organization alone could be isolated from other confounding features. We thus studied a case where the network begins connected, but in a random, disorganized arrangement, and then allowed the system to self-organize under the constraint of *fixed* total density and also binary and undirected connectivity. Together, these conditions mean that only a fraction of the nodes can be directly connected at a given time, and the goal is to understand if simple *rearrangements* in those connections, based on a local rule for determining the rewiring, can enhance synchronizability. Thus, the path to a more coherent state is different here than in previous studies on co-evolutionary Kuramoto systems.

Of course, there are still some methodological considerations to make note of, as well as several possibilities for future work. For example, we studied an adaptive mechanism that utilized only local information of a given node, and that preserved binary connectivity and the total number of edges, so as to isolate the effects of rearrangements in network topology from other factors. However, incorporating these constraints required that there be a random component to the rewiring process, and there was not a natural or self-employed stopping condition for network reconfiguration. One could thus further explore numerically how results are affected by the length of time the system is allowed to co-evolve. Other parameters that may be interesting to examine more in depth are the mean degree, the spread in the intrinsic frequencies, and the time-scale of the adaptation in the network. In addition, while some stochasticity or noise is likely a realistic feature of natural systems, it would be interesting to incorporate that into a related adaptation model that allows for weighted rather than binary connectivity between network units. Also, since this study provides only numerical findings and observations, it would be useful to try and understand the results from a more fundamental and analytical standpoint. Finally, we note that continued investigation into the role of network topology and adaptation in shaping dynamics and structure may lead to a better understanding of the development and function of real-world networks, such as neuronal assemblies or large-scale brain structure and activity patterns [5–11]. Indeed, there are many computational models of these systems in which this can be studied [119–122]. In addition, for neural systems in particular, it is interesting to note that while synchronization is often a desired property, hyper-synchronization can also be detrimental, as is the case with epileptic seizures [123]. Therefore, further examination of the tradeoff and transition between local and global synchrony in biologically motivated models [124, 125] – and understanding how this might occur adaptively over time and influence the structure and function of a network – continues to be an exciting line of study.

In conclusion, understanding the concurrent influence of network architecture on the emergence of collective dy-

namics [2–4, 21, 22], and in turn, the effect of a dynamical process on reshaping or inducing network structure [74–76], is currently an active area of research across a broad set of disciplines, including the physical, social, and biological sciences. Along these lines, we have studied a dynamical rewiring scheme for networks of Kuramoto oscillators. The adaptive rule for the network was specifically inspired by previous work on optimizing networks for synchronization of heterogeneous oscillators [64, 65, 69–71, 110–116], from which we wished to uncover how such collective behavior and organization could occur through a self-organizing process. We found that a restructuring of the network, in which the effect of incoherence is suppressed by maintaining edges between disparate oscillators, while randomly rewiring edges between the most locally and instantaneously in-phase oscillators, led to the emergence of distinct topological patterns and correlations that concurrently enhance the system’s ability to synchronize. This study thus sheds light on a mechanism for how enhanced synchronization and network structure might arise in a system that evolves according to local information alone, without knowledge of global connectivity or node states.

## VI. ACKNOWLEDGMENTS

L.P. acknowledges support from the National Science Foundation Graduate Research Fellowship Program. J.K. acknowledges support from the National Science Foundation Graduate Research Fellowship Program and NIH T32-EB020087, PD: Felix W. Wehrli. D.S.B. also acknowledges support from the John D. and Catherine T. MacArthur Foundation, the Alfred P. Sloan Foundation, and the National Science Foundation (BCS-1441502, CAREER PHY-1554488, BCS-1631550, and CNS-1626008). The content is solely the responsibility of the authors and does not necessarily represent the official views of any of the funding agencies.

## Appendix A: An additional measure to quantify relationships between network topology and oscillator frequencies

In Sec. IV B, we used two measures to quantify the emerging relationships between the intrinsic frequencies of the oscillators and the network topology: the correlation  $C_{|\tilde{\omega}|,k}$  between oscillator frequency offset  $\tilde{\omega}_i$  and the node degree  $k_i$ , and the fraction  $f$  of an oscillator's neighbors that have natural frequency offsets of opposite sign compared to the given oscillator (averaged across all nodes in the system) [64, 65]. Here we define a related measure to further understand the organization that arises in the rewired networks. In particular, we assess the association between the frequency offsets of each node and the *sum* of a node's neighbors' frequency offsets. We quantify this relationship by considering the correlation  $C_{\tilde{\omega},\sum\tilde{\omega}}$  between  $\tilde{\omega}_i$  and  $\sum_{j \in \mathcal{N}(i)} \tilde{\omega}_j$ .

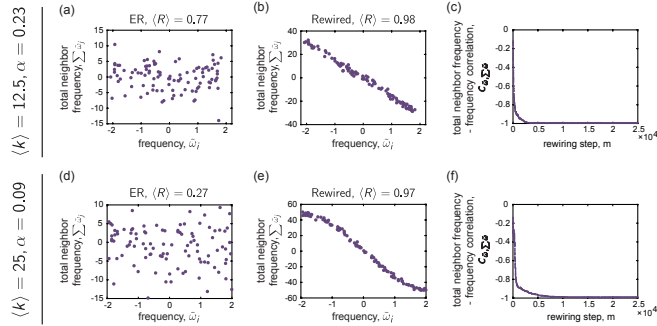


FIG. 11. The relationship between the oscillator frequency offset  $\tilde{\omega}_i$  and the sum of neighbor frequency offsets  $\sum \tilde{\omega}_j$  can be used to further quantify the interplay between the network structure and the intrinsic frequencies of the oscillators that arises due to the co-evolutionary process. The top two rows show examples of this relationship for a network with  $\langle k \rangle = 12.5$ , and the bottom two rows show examples for a network with  $\langle k \rangle = 25$ ; in both cases, the frequencies were drawn from the uniform distribution  $\{\omega_U\}$ . For each network density, the first column corresponds to an ER random graph that exhibits only intermediate levels of synchrony (as measured by  $\langle R \rangle$ ) at the displayed coupling  $\alpha$ , and the second column corresponds to the adapted network, which exhibits a higher level of synchrony. (a,b); (d,e) The total neighbor frequency offset  $\sum \tilde{\omega}_j$  vs. frequency offset  $\tilde{\omega}_i$ . (c); (f) The correlation  $C_{\tilde{\omega},\sum\tilde{\omega}}$  between oscillator frequency offset  $\tilde{\omega}_i$  and the sum of neighbor frequency offsets  $\sum \tilde{\omega}_j$  vs. the number of rewiring steps  $m$ .

Fig. 11 gives examples of this relationship for the same networks as those in Fig. 4 in the main text (the top and bottom rows correspond networks with  $\langle k \rangle = 12.5$  and  $\langle k \rangle = 25$ , respectively). Panels (a); (d) show that in the ER networks, there is no clear relationship between frequency offset and the sum of neighbor frequency offsets, as expected. In the adaptively rewired networks (panels (b); (e)) - for which the order parameter has increased from its original value - there is a strong negative correlation between  $\tilde{\omega}_i$  and  $\sum_{j \in \mathcal{N}(i)} \tilde{\omega}_j$ . So not only do connec-

tions tend to form between oscillators with opposite frequency offset signs (as measured by  $f$ ), but in addition, edges become distributed in the network such that the sum of each oscillator's neighbor frequency offsets proportionately cancels out each oscillator's own difference from the mean frequency of the population. Fig. 11c,f shows how the strength of this relationship - quantified by the correlation  $C_{\tilde{\omega},\sum\tilde{\omega}}$  - evolves as the network is rewired.

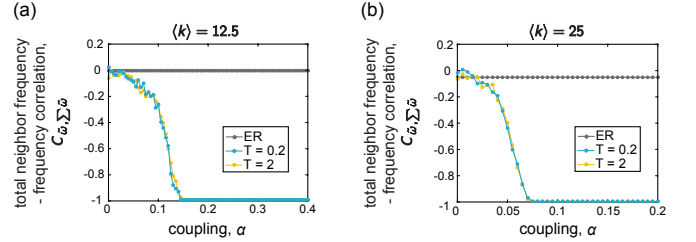


FIG. 12. These plots depict the correlation  $C_{\tilde{\omega},\sum\tilde{\omega}}$  between oscillator frequency offset  $\tilde{\omega}_i$  and the sum of neighbor frequency offsets  $\sum \tilde{\omega}_j$ , as a function of the coupling. In each panel, the blue data points correspond to the initial, uncorrelated ER random graphs  $\mathcal{G}_o$ , and the orange and yellow points correspond to the adapted networks  $\mathcal{G}_*$  evolved under rewiring time scales of  $T = 0.2$  and  $T = 2$ , respectively. The frequencies were drawn from the uniform distribution  $\{\omega_U\}$ , and the mean degree of the networks are (a)  $\langle k \rangle = 12.5$ , and (b)  $\langle k \rangle = 25$ . All curves depict averages over 25 instantiations, and the lines between data points serve as guides for the eye.

Fig. 12 shows  $C_{\tilde{\omega},\sum\tilde{\omega}}$  as a function of the coupling  $\alpha$ . As  $\alpha$  increases,  $C_{\tilde{\omega},\sum\tilde{\omega}}$  decreases to a strong negative value, and then remains approximately constant for larger values of the coupling. The other measures,  $C_{|\tilde{\omega}|,k}$  and  $f$ , exhibit similar types of transitions (see Fig. 5 and Fig. 6). Finally, note that the strong decreases in  $C_{\tilde{\omega},\sum\tilde{\omega}}$  occur in conjunction with increases in the order parameter (Fig. 3).

## Appendix B: Analysis with normally distributed frequencies

The analysis in the main text was carried out using natural frequencies  $\{\omega_U\}$  drawn at random from the uniform distribution in the range  $[-2, 2]$ . In this Appendix, we also consider the case of frequencies  $\{\omega_G\}$  drawn from a normal distribution with zero mean and unit standard deviation. Most of the results shown here are consistent with those in the main text, but we also point out some differences that could be interesting to examine further in future work.

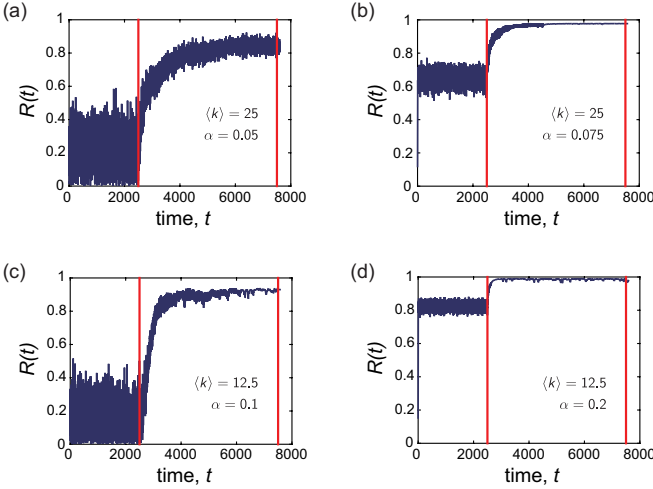


FIG. 13. Examples of the global order parameter  $R(t)$  vs. time  $t$ , for various representative couplings  $\alpha$ . In each case, the dynamics were first run atop an initially ER random graph with average degree  $\langle k \rangle$ , after which co-evolution of the network and dynamics took place between the two red lines. The natural frequencies were drawn from a normal distribution  $\{\omega_G\}$ , and the mean degree  $\langle k \rangle$  and coupling  $\alpha$  used for each panel were (a)  $\langle k \rangle = 25$ ,  $\alpha = 0.05$ , (b)  $\langle k \rangle = 25$ ,  $\alpha = 0.075$ , (c)  $\langle k \rangle = 12.5$ ,  $\alpha = 0.1$ , (d)  $\langle k \rangle = 12.5$ ,  $\alpha = 0.2$ . During the adaptation period, the network was continually rewired once every  $T = 0.2$  time units. The co-evolving networks exhibit enhanced collective dynamics, as observed by increases in the global order parameter.

### 1. Dependence of the order parameter on time and global coupling

Fig. 13 shows examples of the order parameter vs. time for the two different network densities and at several values of the coupling. For these trials and values of the coupling, we observe that the order parameter increases due to the rewiring of the network, which takes place between the two red lines.

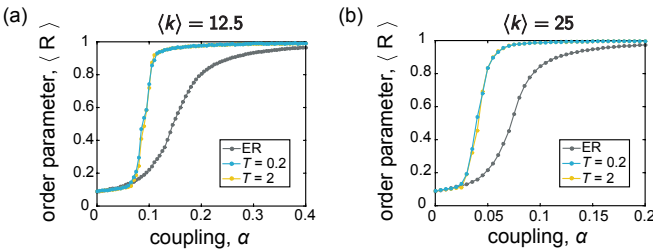


FIG. 14. The time-averaged order parameter vs. coupling. In each panel, the gray data points correspond to static ER random graphs  $\mathcal{G}_o$ , and the blue and yellow points correspond to the adapted networks  $\mathcal{G}_*$  evolved under rewiring time scales of  $T = 0.2$  and  $T = 2$ , respectively. The frequencies were drawn from the normal distribution  $\{\omega_G\}$ , and the mean degree of the networks were (a)  $\langle k \rangle = 12.5$ , and (b)  $\langle k \rangle = 25$ . All curves depict averages over 25 instantiations, and the lines between data points serve as guides for the eye.

Fig. 14 shows examples of the time-averaged order parameter vs. coupling. As with the case of uniformly distributed frequencies (Fig. 3), we find that the adapted networks exhibit heightened synchronization over a large coupling range.

## 2. Correlations with the intrinsic frequencies

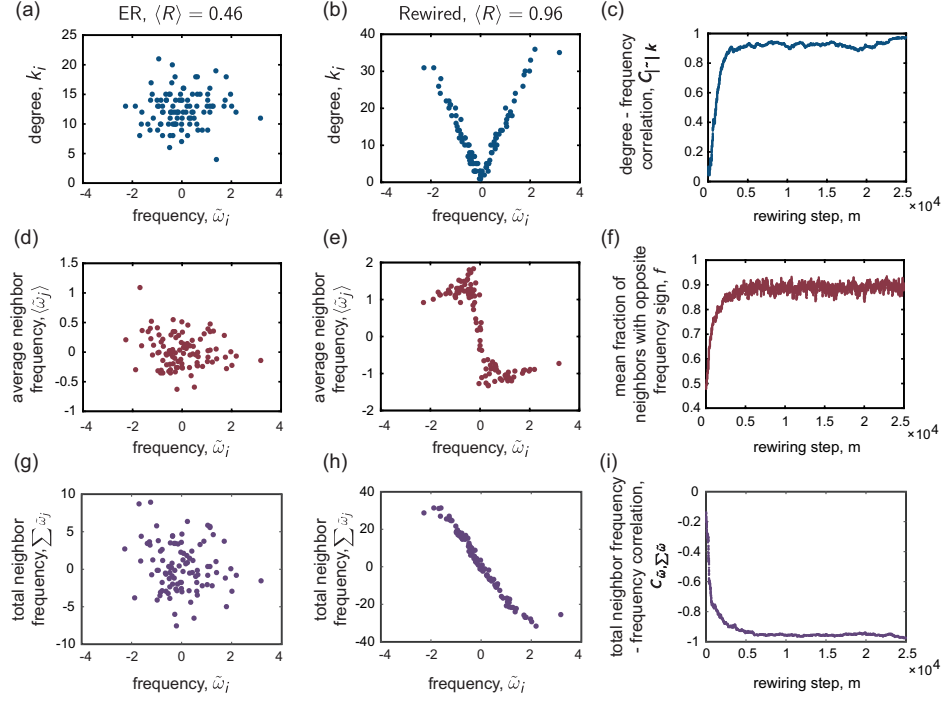
For the case of normally distributed frequencies  $\{\omega_G\}$ , Fig. 15 shows examples of node degree  $k_i$  vs. intrinsic frequency offset  $\tilde{\omega}_i$ , average neighbor frequency offset  $\langle \tilde{\omega}_j \rangle$  vs. node frequency offset  $\tilde{\omega}_i$ , and total neighbor frequency offset  $\sum \tilde{\omega}_j$  vs. frequency offset  $\tilde{\omega}_i$  for ER networks and the corresponding co-evolved networks (Sec. IV B and Appendix A). The top three and bottom three panels correspond to networks with  $\langle k \rangle = 12.5$  and  $\langle k \rangle = 25$ , respectively. At the values of coupling used for these examples, we see that as the system reconfigures, the network begins to exhibit distinct patterns in terms of the organization of oscillators with different intrinsic frequencies. Each of the three metrics considered -  $C_{|\tilde{\omega}|,k}$ ,  $f$ , and  $C_{\tilde{\omega}, \sum \tilde{\omega}}$  - exhibits a progression that allows for the eventual heightened degree of synchrony in the rewired network. These findings are similar to those discussed for the uniform frequency distribution (see Figs. 4 and 11 and the corresponding text).

We next show the evolution of the relationships between network topology and the intrinsic frequencies as a function of the coupling  $\alpha$ . Figs. 16, 17, and 18 show  $C_{|\tilde{\omega}|,k}$  vs.  $\alpha$ ,  $f$  vs.  $\alpha$ , and  $C_{\tilde{\omega}, \sum \tilde{\omega}}$  vs.  $\alpha$ , respectively. The conclusions drawn for the case of normally distributed frequencies shown here are the same as those for the uniformly distributed frequencies examined in the main text. See Figs. 5, 6, and 12 and the corresponding discussions in Sec. IV B and Appendix A). Briefly, each of the three measures exhibit transitions at similar values of the coupling, and the emergence of strong relationships arise near the coupling when the order parameter transitions from low to higher values.

## 3. Analysis of the time-dependence of the adaptive mechanism

We next consider the evolution of the instantaneous frequencies  $\dot{\theta}_i(t)$  vs. time, for different values of the coupling  $\alpha$ . In Fig. 19, each row corresponds to one oscillator, and they are ordered by the quantity  $\tilde{\omega}_i = \omega_i - \langle \omega \rangle$ . The time period over which the network is dynamically adapting is denoted by the black lines. When the coupling is very low, the adaptive mechanism has little effect. At intermediate values of  $\alpha$ , there is first a time-lag during which it is difficult to discern a consistent transformation in the evolution of the instantaneous frequencies, even though the system is co-evolving. After this delay, which appears to shorten as the coupling increases,

$$\langle k \rangle = 12.5, \alpha = 0.13$$



$$\langle k \rangle = 25, \alpha = 0.08$$

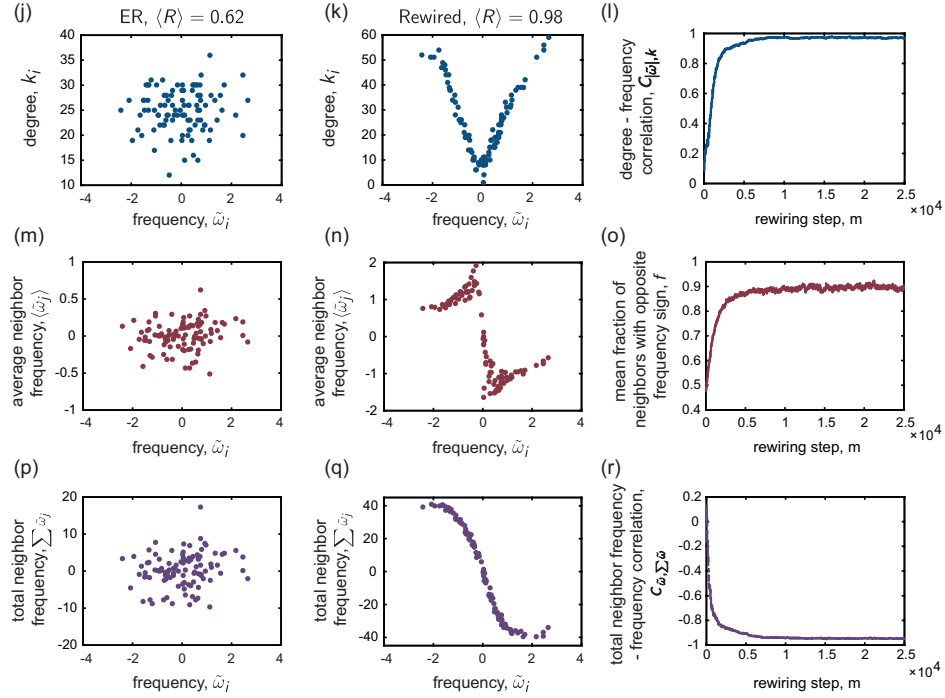


FIG. 15. Relationships between the network structure and the intrinsic frequencies of the oscillators. The top two rows show examples for a network with  $\langle k \rangle = 12.5$ , and the bottom two rows show examples for a network with  $\langle k \rangle = 25$ ; in both cases, the frequencies were drawn from the normal distribution  $\{\omega_G\}$ . For each network density, the first column corresponds to an ER random graph that exhibits only intermediate levels of synchrony (as measured by  $\langle R \rangle$ ) at the displayed coupling  $\alpha$ , and the second column corresponds to the adapted network, which exhibits a higher level of synchrony. These plots highlight key relationships that emerge from the co-evolutionary network update rule. (a,b); (j,k) Node degree  $k_i$  vs. frequency offset  $\tilde{\omega}_i$ . (d,e); (m,n) Average neighbor frequency offset  $\langle \tilde{\omega}_j \rangle$  vs. frequency offset  $\tilde{\omega}_i$ . (g,h); (p,q) Total neighbor frequency offset  $\sum \tilde{\omega}_j$  vs. frequency offset  $\tilde{\omega}_i$ . (c); (l) The correlation  $C_{|\tilde{\omega}_i|, k}$  between node degree  $k_i$  and the magnitude of the frequency offset  $\tilde{\omega}_i$  vs. the number of rewiring steps  $m$ , and (f); (o) the fraction  $f$  of an oscillator's neighbors that have frequency offsets of opposite sign compared to the given oscillator (averaged over all nodes in the network) vs. the number of rewiring steps  $m$ . (i); (r) The correlation  $C_{\tilde{\omega}_i, \sum \tilde{\omega}_j}$  between oscillator frequency offset  $\tilde{\omega}_i$  and the sum of neighbor frequency offsets  $\sum \tilde{\omega}_j$  vs. the number of rewiring steps  $m$ .

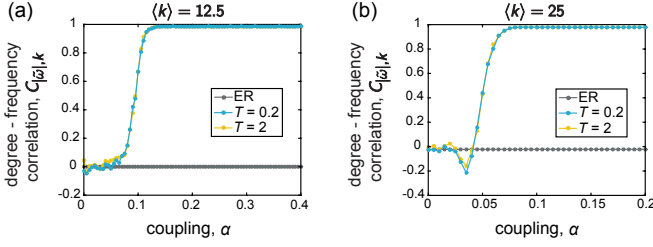


FIG. 16. These plots depict the correlation  $C_{|\tilde{\omega}|,k}$  between node degree  $k_i$  and the magnitude of the frequency offset  $|\tilde{\omega}_i|$ , as a function of the coupling. In each panel, the blue data points correspond to the initial, uncorrelated ER random graphs  $\mathcal{G}_o$ , and the orange and yellow points correspond to the adapted networks  $G_*$  evolved under rewiring time scales of  $T = 0.2$  and  $T = 2$ , respectively. The frequencies were drawn from the normal distribution  $\{\omega_G\}$ , and the mean degree of the networks are (a)  $\langle k \rangle = 12.5$ , and (b)  $\langle k \rangle = 25$ . The dip observed in (b) at  $\alpha \approx 0.4$  is due to the localization of edges on a cluster of oscillators with natural frequencies near the mean; this is examined further in Sec. B 3. All curves depict averages over 25 instantiations, and the lines between data points serve as guides for the eye.

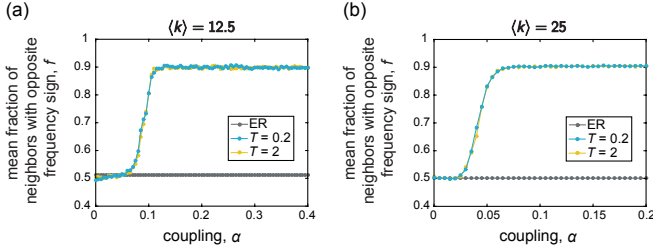


FIG. 17. These plots depict the mean fraction  $f$  of an oscillator's neighbors that have natural frequency offsets of opposite sign compared to that of the given oscillator, as a function of the coupling. In each panel, the blue data points correspond to the initial, uncorrelated ER random graphs  $\mathcal{G}_o$ , and the orange and yellow points correspond to the adapted networks  $G_*$  evolved under rewiring time scales of  $T = 0.2$  and  $T = 2$ , respectively. The frequencies were drawn from the normal distribution  $\{\omega_G\}$ , and the mean degree of the networks are (a)  $\langle k \rangle = 12.5$ , and (b)  $\langle k \rangle = 25$ . All curves depict averages over 25 instantiations, and the lines between data points serve as guides for the eye.

we begin to see a change in behavior. When the coupling is still low enough (for example,  $\alpha = 0.0875$ ) we observe similar behavior to the examples using the uniform frequency distribution (Fig. 7); first oscillators with intrinsic frequencies closer to the mean synchronize, followed by oscillators with natural frequencies more on the edge of the distribution. As the coupling increases, this dependence on the intrinsic frequency becomes less distinguishable, and the transition evoked by the adaptive mechanism is more rapid.

Finally, we examine the time-evolution of the relationship between node degree and intrinsic frequency. Fig. 20 shows examples of the node degree  $k_i$  vs. the rewiring

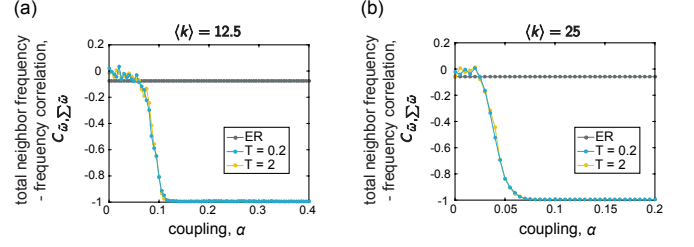


FIG. 18. These plots depict the correlation  $C_{\tilde{\omega},\Sigma\tilde{\omega}}$  between oscillator frequency offset  $\tilde{\omega}_i$  and the sum of neighbor frequency offsets  $\Sigma\tilde{\omega}_j$ , as a function of the coupling. In each panel, the blue data points correspond to the initial, uncorrelated ER random graphs  $\mathcal{G}_o$ , and the orange and yellow points correspond to the adapted networks  $G_*$  evolved under rewiring time scales of  $T = 0.2$  and  $T = 2$ , respectively. The frequencies were drawn from the normal distribution  $\{\omega_G\}$ , and the mean degree of the networks are (a)  $\langle k \rangle = 12.5$ , and (b)  $\langle k \rangle = 25$ . All curves depict averages over 25 instantiations, and the lines between data points serve as guides for the eye.

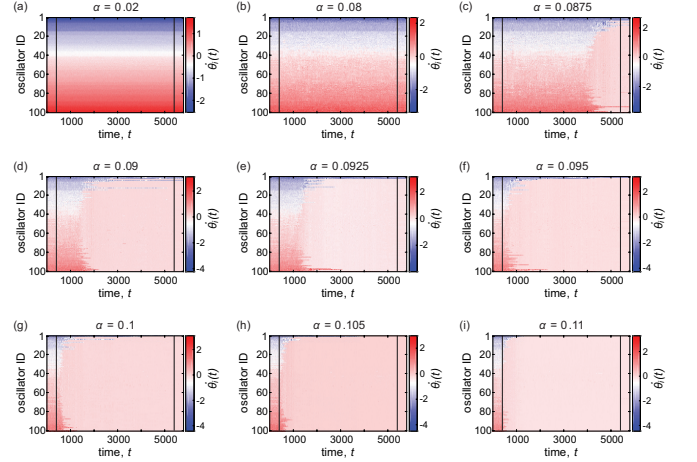


FIG. 19. Examples of the instantaneous frequencies  $\hat{\theta}_i(t)$  vs. time  $t$ , for various representative couplings  $\alpha$ . Each row corresponds to one oscillator, and the rows are ordered by the quantity  $\tilde{\omega}_i = \omega_i - \langle \omega \rangle$  (i.e. the offset from the mean intrinsic frequency of the population). In each case, the dynamics were first run atop an initially ER random graph, after which co-evolution of the network and dynamics took place between the two black lines. For these plots, the natural frequencies were drawn from the normal distribution  $\{\omega_G\}$  and the mean degree of the network was  $\langle k \rangle = 12.5$ . During the adaptation period, the network was continually rewired once every  $T = 0.2$  time units.

step  $m$  (as before, the rows are ordered by  $\tilde{\omega}_i$  and Fig. 21 depicts the corresponding evolution of the correlation  $C_{|\tilde{\omega}|,k}$  between the magnitude of the frequency offset  $|\tilde{\omega}_i|$  and the degree  $k_i$ . For all values of the coupling shown here,  $C_{|\tilde{\omega}|,k}$  remains fluctuating around zero, and then increases to a positive value if the coupling is high enough. This behavior is consistent with the examples shown for the uniform frequency distribution and  $\langle k \rangle = 12.5$  (Fig. 8

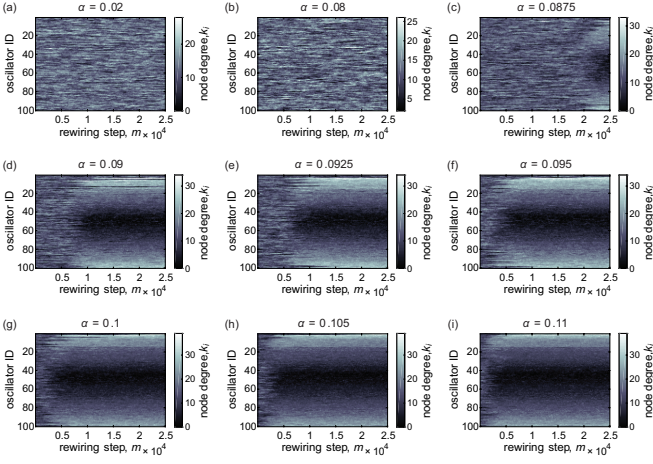


FIG. 20. Examples of the evolution of the node degree  $k_i$  vs. the rewiring step  $m$ , for various representative couplings  $\alpha$ . Each row corresponds to one oscillator, and the rows are ordered by the quantity  $\tilde{\omega}_i = \omega_i - \langle \omega \rangle$  (i.e. the offset from the mean intrinsic frequency of the population). For these plots, the natural frequencies were drawn from the normal distribution  $\{\omega_G\}$  and the mean degree of the network was  $\langle k \rangle = 12.5$ , and the network was continually rewired once every  $T = 0.2$  time units.

and Fig. 9).

#### 4. Spectral Analysis

In Sec. IVD we carried out a spectral-based analysis of the co-evolved networks inspired by [69]. In the main text we examined the case of uniformly distributed frequencies  $\{\omega_U\}$  (see Fig. 10); here in Fig. 22 we also show the results for the case of normally distributed frequencies  $\{\omega_G\}$ , which are consistent with those previously discussed. In short, for both values of the mean degree ( $\langle k \rangle = 12.5$  and  $\langle k \rangle = 25$ ) the overlap  $|\langle \frac{\tilde{\omega}}{\|\tilde{\omega}\|}, \frac{\mathbf{v}_N}{\|\mathbf{v}_N\|} \rangle|$  between the normalized natural frequency offsets and the normalized dominant Laplacian eigenvector of the rewired networks increases and then plateaus at a high value as the coupling increases (Fig. 22a,b). Concurrently, the largest and smallest eigenvalues of the Laplacian increase and decrease, respectively, as a function of increasing coupling (Fig. 22c, d). We refer the reader to Sec. IVD for a more detailed discussion of these findings.

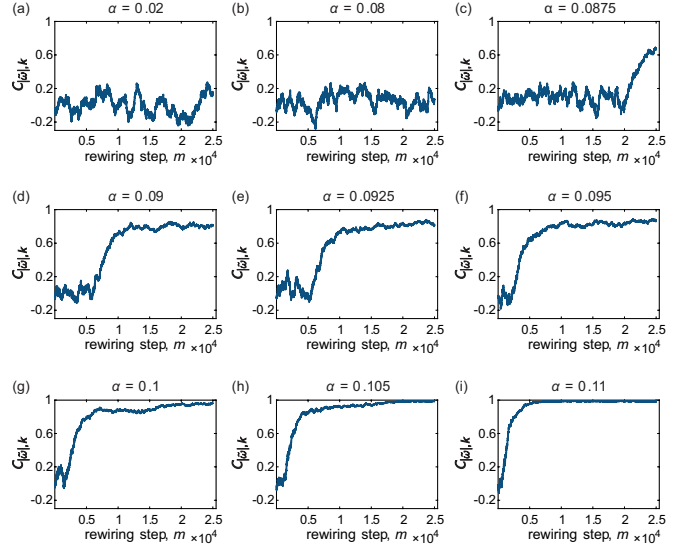


FIG. 21. Examples of the evolution of the correlation  $C_{|\tilde{\omega}|,k}$  between oscillator frequency offset  $\tilde{\omega}_i$  and the node degree  $k_i$ , vs. the rewiring step  $m$ , for various representative couplings  $\alpha$ . For these plots, the natural frequencies were drawn from the normal distribution  $\{\omega_G\}$  and the mean degree of the network was  $\langle k \rangle = 12.5$ , and the network was continually rewired once every  $T = 0.2$  time units.

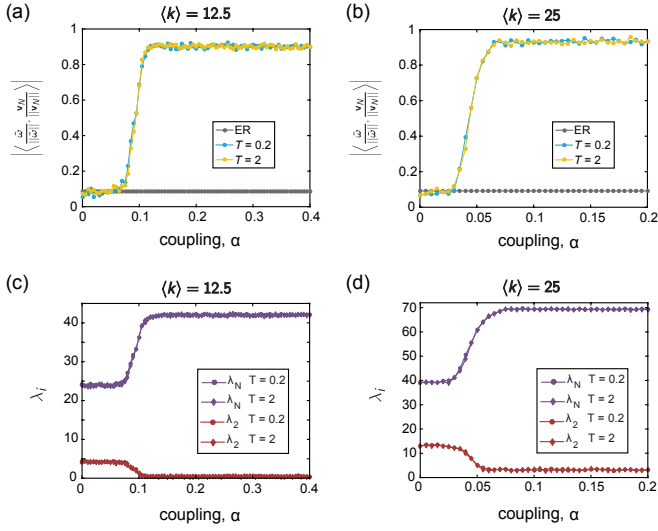


FIG. 22. A spectral analysis of the adaptively rewired networks. (a, b) Evolution of the overlap  $\left\langle \frac{\tilde{\omega}}{\|\tilde{\omega}\|}, \frac{\mathbf{v}_N}{\|\mathbf{v}_N\|} \right\rangle$  between the intrinsic frequencies  $\tilde{\omega}$  and dominant Laplacian eigenvector  $\mathbf{v}_N$  as a function of the coupling. In each panel, the gray data points correspond to the original, uncorrelated ER random graphs  $\mathcal{G}_o$ , and the blue and yellow curves correspond to the adapted networks  $\mathcal{G}_*$  evolved under rewiring time scales of  $T = 0.2$  and  $T = 2$ , respectively. (c, d) Evolution of the first non-zero eigenvalue  $\lambda_2$  (maroon data) and the largest eigenvalue  $\lambda_N$  (purple data) of the Laplacian  $\mathbf{L}$  as a function of the coupling. In each panel, the eigenvalues were computed on the final adapted networks  $\mathcal{G}_*$  evolved under rewiring time scales of  $T = 0.2$  (circles) and  $T = 2$  (diamonds). The natural frequencies were drawn from the normal distribution  $\{\omega_G\}$ , and the mean degree  $\langle k \rangle$  of the networks are (a, c)  $\langle k \rangle = 12.5$ ; (b, d)  $\langle k \rangle = 25$ . All curves depict averages over 25 instantiations, and the lines between data points serve as guides for the eye.

- 
- [1] M. E. J. Newman, *SIAM Review* **45**, 167 (2003).
- [2] S. Boccaletti, V. Latora, Y. Moreno, M. Chavez, and D.-U. Hwang, *Physics Reports* **424**, 175 (2006).
- [3] M. Barthelemy, A. Barrat, and A. Vespignani, *Dynamical processes on complex networks* (Cambridge University Press, 2008).
- [4] A. Vespignani, *Nat Phys* **8**, 32 (2012).
- [5] G. B. Ermentrout and D. H. Terman, *Mathematical foundations of neuroscience* (Springer-Verlag, 2010).
- [6] N. Brunel and V. Hakim, *Neural computation* **11**, 1621 (1999).
- [7] N. Brunel, *Journal of Computational Neuroscience* **8**, 183 (2000).
- [8] X. Guardiola, A. Díaz-Guilera, M. Llas, and C. J. Pérez, *Phys. Rev. E* **62**, 5565 (2000).
- [9] L. F. Lago-Fernández, R. Huerta, F. Corbacho, and J. A. Sigüenza, *Phys. Rev. Lett.* **84**, 2758 (2000).
- [10] M. Denker, M. Timme, M. Diesmann, F. Wolf, and T. Geisel, *Phys. Rev. Lett.* **92**, 074103 (2004).
- [11] A. Roxin, H. Riecke, and S. A. Solla, *Phys. Rev. Lett.* **92**, 198101 (2004).
- [12] D. S. Bassett, D. L. Alderson, and J. M. Carlson, *Phys Rev E Stat Nonlin Soft Matter Phys* **86**, 036105 (2012).
- [13] J. C. Miller and I. Z. Kiss, *Mathematical Modelling of Natural Phenomena* **9**, 4 (2014).
- [14] R. Pastor-Satorras, C. Castellano, P. Van Mieghem, and A. Vespignani, *Rev. Mod. Phys.* **87**, 925 (2015).
- [15] Y. Moreno, R. Pastor-Satorras, and A. Vespignani, *The European Physical Journal B - Condensed Matter and Complex Systems* **26**, 521 (2002).
- [16] A.-L. Barabasi and Z. N. Oltvai, *Nat Rev Genet* **5**, 101 (2004).
- [17] G. Karlebach and R. Shamir, *Nat Rev Mol Cell Biol* **9**, 770 (2008).
- [18] M. B. Elowitz and S. Leibler, *Nature* **403**, 335 (2000).
- [19] N. M. Luscombe, M. Madan Babu, H. Yu, M. Snyder, S. A. Teichmann, and M. Gerstein, *Nature* **431**, 308 (2004).
- [20] C. M. Henzler, Z. Li, J. Dang, M. L. Arcila, H. Zhou, J. Liu, K. Y. Chang, D. S. Bassett, T. M. Rana, and K. S. Kosik, *Genome Biol* **14**, R149 (2013).
- [21] A. T. Winfree, *The geometry of biological time* (Springer Verlag, 1980).
- [22] S. Strogatz, *Sync: The Emerging Science of Spontaneous Order* (Hyperion Press, 2003).
- [23] A. Pikovsky, M. Rosenblum, and J. Kurths, *Synchronization: a universal concept in nonlinear sciences* (Cambridge university press, 2003).
- [24] S. C. Manrubia, A. S. Mikhailov, and D. H. Zanette, *Emergence of dynamical order: synchronization phenomena in complex systems* (World Scientific, 2004).
- [25] A. Arenas, A. Díaz-Guilera, J. Kurths, Y. Moreno, and C. Zhou, *Physics Reports* **469**, 93 (2008).
- [26] L. Glass, *Nature* **410**, 277 (2001).
- [27] P. Fries, *Trends in Cognitive Sciences* **9**, 474 (2005).
- [28] D. S. Bassett, A. Meyer-Lindenberg, S. Achard, T. Duke, and E. T. Bullmore, *Proc Natl Acad Sci U S A* **103**, 19518 (2006).
- [29] A. N. Khambhati, K. A. Davis, B. S. Oommen, S. H. Chen, T. H. Lucas, B. Litt, and D. S. Bassett, *PLOS Computational Biology* **11**, e1004608 (2015).
- [30] F. Siebenhühner, S. A. Weiss, R. Coppola, D. R. Weinberger, and D. S. Bassett, *PLOS ONE* **8**, 1 (2013).
- [31] D. S. Bassett, E. T. Bullmore, A. Meyer-Lindenberg, J. A. Apud, D. R. Weinberger, and R. Coppola, *Proc Natl Acad Sci U S A* **106**, 11747 (2009).
- [32] O. Sporns, G. Tononi, and G. Edelman, *Neural Networks* **13**, 909 (2000).
- [33] C. J. Stam, *Neuroscience Letters* **355**, 25 (2004).
- [34] N. Kopell, G. B. Ermentrout, M. A. Whittington, and R. D. Traub, *Proceedings of the National Academy of Sciences* **97**, 1867 (2000).
- [35] A. K. Engel, P. Fries, and W. Singer, *Nat Rev Neurosci* **2**, 704 (2001).
- [36] M. D. Fox, A. Z. Snyder, J. L. Vincent, M. Corbetta, D. C. Van Essen, and M. E. Raichle, *Proceedings of the National Academy of Sciences of the United States of America* **102**, 9673 (2005).
- [37] G. Buzsáki and A. Draguhn, *Science* **304**, 1926 (2004).
- [38] F. Varela, J.-P. Lachaux, E. Rodriguez, and J. Martinerie, *Nat Rev Neurosci* **2**, 229 (2001).
- [39] S. Lozano, L. Buzna, and A. Díaz-Guilera, *The European Physical Journal B* **85**, 231 (2012).
- [40] F. Dörfler and F. Bullo, *SIAM Journal on Control and Optimization* **50**, 1616 (2012).
- [41] M. Rohden, A. Sorge, M. Timme, and D. Witthaut, *Phys. Rev. Lett.* **109**, 064101 (2012).
- [42] A. E. Motter, S. A. Myers, M. Anghel, and T. Nishikawa, *Nat Phys* **9**, 191 (2013).
- [43] Y. Kuramoto, in *International symposium on mathematical problems in theoretical physics*, Lecture Notes in Physics, Vol. 39, edited by H. Araki (Springer, 1975) pp. 420–422.
- [44] Y. Kuramoto, *Chemical Oscillations, Waves, and Turbulence Chemical Oscillations, Waves, and Turbulence* (Springer-Verlag, 1984).
- [45] S. H. Strogatz, *Physica D: Nonlinear Phenomena* **143**, 1 (2000).
- [46] J. A. Acebrón, L. L. Bonilla, C. J. Pérez Vicente, F. Ritort, and R. Spigler, *Rev. Mod. Phys.* **77**, 137 (2005).
- [47] F. A. Rodrigues, T. K. D. Peron, P. Ji, and J. Kurths, *Physics Reports* **610**, 1 (2016).
- [48] A.-L. Barabási and R. Albert, *Science* **286**, 509 (1999).
- [49] Y. Moreno and A. F. Pacheco, *EPL (Europhysics Letters)* **68**, 603 (2004).
- [50] D.-S. Lee, *Phys. Rev. E* **72**, 026208 (2005).
- [51] J. Gómez-Gardeñes, Y. Moreno, and A. Arenas, *Phys. Rev. E* **75**, 066106 (2007).
- [52] J. Gómez-Gardeñes, Y. Moreno, and A. Arenas, *Phys. Rev. Lett.* **98**, 034101 (2007).
- [53] D. J. Watts and S. H. Strogatz, *Nature* **393**, 440 (1998).
- [54] H. Hong, M. Y. Choi, and B. J. Kim, *Phys. Rev. E* **65**, 026139 (2002).
- [55] M. E. J. Newman, *Proceedings of the National Academy of Sciences* **103**, 8577 (2006).
- [56] E. Oh, K. Rho, H. Hong, and B. Kahng, *Phys. Rev. E* **72**, 047101 (2005).
- [57] A. Arenas, A. Díaz-Guilera, and C. J. Pérez-Vicente, *Phys. Rev. Lett.* **96**, 114102 (2006).
- [58] A. Arenas and A. Díaz-Guilera, *The European Physical Journal Special Topics* **143**, 19 (2007).

- [59] A. Arenas, A. Díaz-Guilera, and C. J. Pérez-Vicente, *Physica D: Nonlinear Phenomena* **224**, 27 (2006), dynamics on Complex Networks and Applications.
- [60] S. Guan, X. Wang, Y.-C. Lai, and C.-H. Lai, *Phys. Rev. E* **77**, 046211 (2008).
- [61] P. S. Skardal and J. G. Restrepo, *Phys. Rev. E* **85**, 016208 (2012).
- [62] L. M. Pecora and T. L. Carroll, *Phys. Rev. Lett.* **80**, 2109 (1998).
- [63] M. Barahona and L. M. Pecora, *Phys. Rev. Lett.* **89**, 054101 (2002).
- [64] M. Brede, *Physics Letters A* **372**, 2618 (2008).
- [65] M. Brede, “Enhancing synchronization in systems of non-identical kuramoto oscillators,” in *Complex Sciences: First International Conference, Complex 2009, Shanghai, China, February 23-25, 2009, Revised Papers, Part 2*, edited by J. Zhou (Springer Berlin Heidelberg, Berlin, Heidelberg, 2009) pp. 1955–1966.
- [66] J. Gómez-Gardeñes, S. Gómez, A. Arenas, and Y. Moreno, *Phys. Rev. Lett.* **106**, 128701 (2011).
- [67] I. Leyva, A. Navas, I. Sendiña-Nadal, J. A. Almendral, J. M. Buldú, M. Zanin, D. Papo, and S. Boccaletti, *Scientific Reports* **3**, 1281 EP (2013).
- [68] I. Leyva, I. Sendiña Nadal, J. A. Almendral, A. Navas, S. Olmi, and S. Boccaletti, *Phys. Rev. E* **88**, 042808 (2013).
- [69] P. S. Skardal, D. Taylor, and J. Sun, *Phys. Rev. Lett.* **113**, 144101 (2014).
- [70] P. S. Skardal, D. Taylor, J. Sun, and A. Arenas, *Phys. Rev. E* **91**, 010802 (2015).
- [71] D. Taylor, P. S. Skardal, and J. Sun, *SIAM Journal on Applied Mathematics* **76**, 1984 (2016).
- [72] G. A. Gottwald, *Chaos: An Interdisciplinary Journal of Nonlinear Science* **25**, 053111 (2015).
- [73] R. S. Pinto and A. Saa, *Phys. Rev. E* **92**, 062801 (2015).
- [74] T. Gross and H. Sayama, *Adaptive networks: Theory, Models and Applications* (Springer, 2009).
- [75] T. Gross and B. Blasius, *Journal of The Royal Society Interface* **5**, 259 (2008).
- [76] H. Sayama, I. Pestov, J. Schmidt, B. J. Bush, C. Wong, J. Yamanoi, and T. Gross, *Computers & Mathematics with Applications* **65**, 1645 (2013).
- [77] W.-J. Yuan and C. Zhou, *Phys. Rev. E* **84**, 016116 (2011).
- [78] W.-J. Yuan, J.-F. Zhou, Q. Li, D.-B. Chen, and Z. Wang, *Phys. Rev. E* **88**, 022818 (2013).
- [79] C. Zhou and J. Kurths, *Phys. Rev. Lett.* **96**, 164102 (2006).
- [80] J.-F. Zhu, M. Zhao, W. Yu, C. Zhou, and B.-H. Wang, *Phys. Rev. E* **81**, 026201 (2010).
- [81] T. Aoki and T. Aoyagi, *Phys. Rev. Lett.* **102**, 034101 (2009).
- [82] T. Aoki and T. Aoyagi, *Phys. Rev. E* **84**, 066109 (2011).
- [83] M. Rubinov, O. Sporns, C. van Leeuwen, and M. Breakspear, *BMC Neuroscience* **10**, 55 (2009).
- [84] P. M. Gleiser and D. H. Zanette, *The European Physical Journal B - Condensed Matter and Complex Systems* **53**, 233 (2006).
- [85] P. Seliger, S. C. Young, and L. S. Tsimring, *Phys. Rev. E* **65**, 041906 (2002).
- [86] I. Sendiña Nadal, I. Leyva, J. M. Buldú, J. A. Almendral, and S. Boccaletti, *Phys. Rev. E* **79**, 046105 (2009).
- [87] I. Sendiña-Nadal, J. M. Buldú, I. Leyva, and S. Boccaletti, *PLOS ONE* **3**, 1 (2008).
- [88] S. Assenza, R. Gutiérrez, J. Gómez-Gardeñes, V. Latora, and S. Boccaletti, *Scientific Reports* **1**, 99 EP (2011).
- [89] R. Gutiérrez, A. Amann, S. Assenza, J. Gómez-Gardeñes, V. Latora, and S. Boccaletti, *Phys. Rev. Lett.* **107**, 234103 (2011).
- [90] H. Markram and M. Tsodyks, *Nature* **382**, 807 (1996).
- [91] S. Song, K. D. Miller, and L. F. Abbott, *Nat Neurosci* **3**, 919 (2000).
- [92] N. Caporale and Y. Dan, *Annual Review of Neuroscience* **31**, 25 (2008).
- [93] K. P. Lamsa, J. H. Heeroma, P. Somogyi, D. A. Rusakov, and D. M. Kullmann, *Science* **315**, 1262 (2007).
- [94] P. D. Roberts and T. K. Leen, *Frontiers in Computational Neuroscience* **4**, 156 (2010).
- [95] T. Gross, C. J. D. D’Lima, and B. Blasius, *Phys. Rev. Lett.* **96**, 208701 (2006).
- [96] P. Holme and M. E. J. Newman, *Phys. Rev. E* **74**, 056108 (2006).
- [97] S. Bornholdt and T. Rohlf, *Phys. Rev. Lett.* **84**, 6114 (2000).
- [98] S. Bornholdt and T. Röhl, *Phys. Rev. E* **67**, 066118 (2003).
- [99] P. Gong and C. van Leeuwen, *EPL (Europhysics Letters)* **67**, 328 (2004).
- [100] F. Sorrentino and E. Ott, *Phys. Rev. Lett.* **100**, 114101 (2008).
- [101] H. F. Kwok, P. Jurica, A. Raffone, and C. van Leeuwen, *Cognitive Neurodynamics* **1**, 39 (2006).
- [102] M. Rubinov, O. Sporns, J.-P. Thivierge, and M. Breakspear, *PLOS Computational Biology* **7**, 1 (2011).
- [103] Q. Ren and J. Zhao, *Phys. Rev. E* **76**, 016207 (2007).
- [104] Q. Ren, M. He, X. Yu, Q. Long, and J. Zhao, *Physics Letters A* **378**, 139 (2014).
- [105] V. Avalos-Gaytán, J. A. Almendral, D. Papo, S. E. Schaeffer, and S. Boccaletti, *Phys. Rev. E* **86**, 015101 (2012).
- [106] L. Timms and L. Q. English, *Phys. Rev. E* **89**, 032906 (2014).
- [107] X. Zhang, S. Boccaletti, S. Guan, and Z. Liu, *Phys. Rev. Lett.* **114**, 038701 (2015).
- [108] R. Singh and T. Bagarti, *Europhysics Letters* **111**, 50010 (2015).
- [109] Y.-H. Eom, S. Boccaletti, and G. Caldarelli, *Scientific Reports* **6**, 27111 EP (2016).
- [110] J. Fan and D. J. Hill, “Enhancement of synchronizability of the kuramoto model with assortative degree-frequency mixing,” in *Complex Sciences: First International Conference, Complex 2009, Shanghai, China, February 23-25, 2009, Revised Papers, Part 2*, edited by J. Zhou (Springer Berlin Heidelberg, Berlin, Heidelberg, 2009) pp. 1967–1972.
- [111] L. Buzna, S. Lozano, and A. Díaz-Guilera, *Phys. Rev. E* **80**, 066120 (2009).
- [112] R. Carareto, F. Orsatti, and J. Piqueira, *Communications in Nonlinear Science and Numerical Simulation* **14**, 2536 (2009).
- [113] D. Kelly and G. A. Gottwald, *Chaos: An Interdisciplinary Journal of Nonlinear Science* **21**, 025110 (2011).
- [114] M. Brede, *Physica D: Nonlinear Phenomena* **239**, 1759 (2010).
- [115] M. Brede, *The European Physical Journal B* **62**, 87 (2008).

- [116] C. Freitas, E. Macau, and R. L. Viana, *Phys. Rev. E* **92**, 032901 (2015).
- [117] See the Supplementary Material at: INSERT URL.
- [118] D. Kimura and Y. Hayakawa, *Phys. Rev. E* **78**, 016103 (2008).
- [119] M. Breakspear, S. Heitmann, and A. Daffertshofer, *Frontiers in Human Neuroscience* **4**, 190 (2010).
- [120] E. M. Izhikevich, *Neural Computation*, *Neural Computation* **18**, 245 (2006).
- [121] N. Jarman, C. Trengove, E. Steur, I. Tyukin, and C. van Leeuwen, *Cognitive Neurodynamics* **8**, 479 (2014).
- [122] G. Deco, V. Jirsa, A. R. McIntosh, O. Sporns, and R. Kötter, *Proceedings of the National Academy of Sciences* **106**, 10302 (2009).
- [123] C. Stam, *Clinical Neurophysiology* **116**, 2266 (2005).
- [124] B. Percha, R. Dzakpasu, M. Żochowski, and J. Parent, *Phys. Rev. E* **72**, 031909 (2005).
- [125] S. Mofakham, C. G. Fink, V. Booth, and M. R. Zochowski, *Phys Rev E* **94**, 042427 (2016).

## Supplementary Information for

## “Development of structural correlations and synchronization from adaptive rewiring in networks of Kuramoto oscillators”

Lia Papadopoulos,<sup>1</sup> Jason Kim,<sup>2</sup> Jürgen Kurths,<sup>3,4,5</sup> and Danielle S. Bassett<sup>2,6</sup><sup>1</sup>*Department of Physics and Astronomy, University of Pennsylvania, Pennsylvania, PA 19104, USA*<sup>2</sup>*Department of Bioengineering, University of Pennsylvania, Pennsylvania, PA 19104, USA*<sup>3</sup>*Potsdam Institute for Climate Impact Research - Telegraphenberg A 31, 14473 Potsdam, Germany*<sup>4</sup>*Department of Physics, Humboldt University Berlin - 12489 Berlin, Germany*<sup>5</sup>*Institute for Complex Systems and Mathematical Biology, University of Aberdeen - Aberdeen AB24 3UE, UK*<sup>6</sup>*Department of Electrical & Systems Engineering, University of Pennsylvania, Pennsylvania, PA 19104, USA\**

(Dated: July 25, 2022)

**I. TIME EVOLUTION OF SYNCHRONIZED CLUSTERS**

The order parameter  $R$  is a global measure of phase synchronization, and when the coupling is high enough, we observe that network adaptation can increase this quantity from a regime that signifies low synchrony to a regime of intermediate to high synchrony. As a supplement to this measure, we can also quantify changes in the system during the adaptation process on a more local level by considering the time-evolution of synchronized clusters of oscillators. For this analysis, we follow [1], who defined a local order parameter between pairs of oscillators as

$$\rho_{ij}(t) = \cos[\theta_i(t) - \theta_j(t)], \quad (1)$$

and then constructed a binarized phase-similarity matrix  $\tilde{\rho}(t)$  by setting any entries less than some threshold  $\Delta$  to zero and by setting any entries greater than  $\Delta$  to 1. Specifically,

$$\tilde{\rho}_{ij}(t) = \begin{cases} 0 & \text{if } \rho_{ij}(t) \leq \Delta \\ 1 & \text{if } \rho_{ij}(t) > \Delta. \end{cases} \quad (2)$$

We use a value of  $\Delta = 0.999$ . The binarized matrix  $\tilde{\rho}(t)$  contains information about which pairs of oscillators are strongly synchronized at a given time, and synchronized *clusters* or groups of oscillators can be extracted by finding the connected components of  $\tilde{\rho}(t)$ . Finally, we can track the number of synchronized components  $n_{sc}(t)$  as a function of time  $t$ , and observe how the behavior in this quantity changes when the network begins to co-evolve with the dynamics. For low values of the coupling - where the adaptive strategy does not appear to have a large influence on the dynamics - we expect  $n_{sc}(t)$  to remain high as a function of time. However when the coupling is increased such that dynamical self-organization

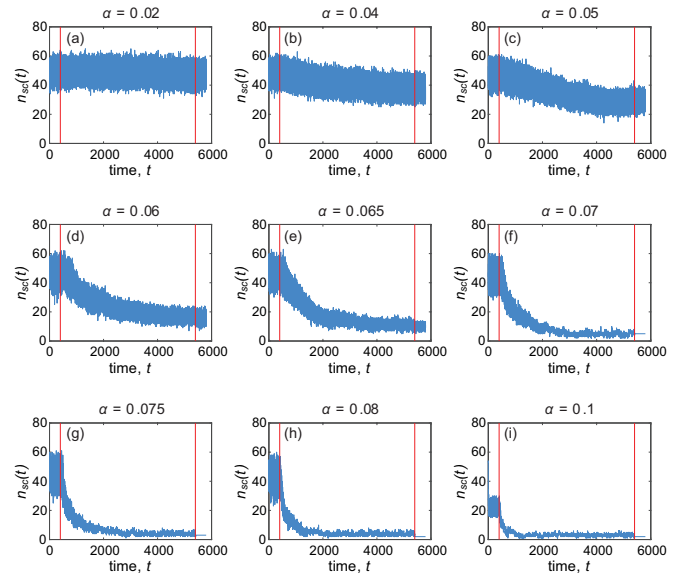


FIG. 1. Examples of the number of synchronized clusters  $n_{sc}(t)$  vs. time  $t$ , for various representative couplings  $\alpha$ . In each case, the dynamics were first run atop an initially ER random graph, after which co-evolution of the network and dynamics took place between the two red lines. For these plots, the natural frequencies were drawn from the uniform distribution  $\{\omega_U\}$  and the mean degree of the network was  $\langle k \rangle = 25$ . During the adaptation period, the network was continually rewired once every  $T = 0.2$  time units. For high enough coupling, co-evolution results in a decrease of the number of synchronized clusters over time.

occurs, we expect a decrease in the number of synchronized components as the network evolves from a configuration that does not support collective dynamics to one that does. An interesting question is whether  $n_{sc}(t)$  decreases in abrupt, sudden bursts, or smoothly over time, and how this behavior depends on the magnitude of the overall coupling  $\alpha$ .

Fig. 1 shows examples of  $n_{sc}(t)$  vs.  $t$  for a single simulation of the dynamics, and for various values of the

\* dsb@seas.upenn.edu

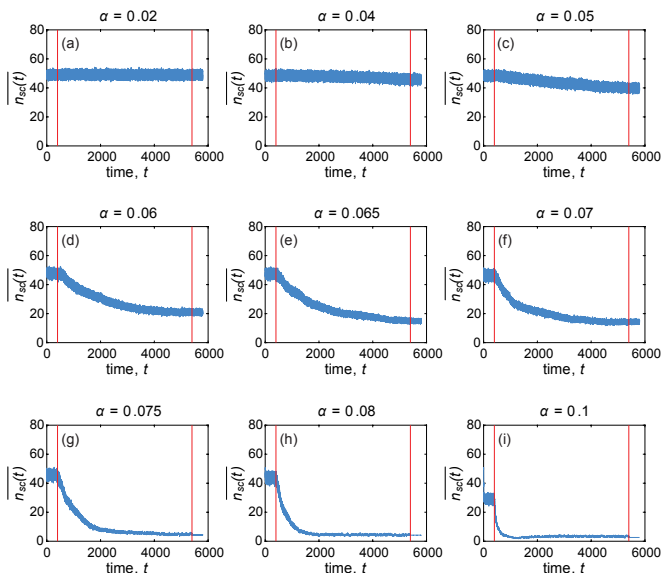


FIG. 2. Ensemble averages of the number of synchronized clusters  $n_{sc}(t)$  vs. time  $t$ , for various representative couplings  $\alpha$ . In each case, the dynamics were first run atop an initially ER random graph, after which co-evolution of the network and dynamics took place between the two red lines. For these plots, the natural frequencies were drawn from the uniform distribution  $\{\omega_U\}$ , the mean degree of the network was  $\langle k \rangle = 25$ , and each curve corresponds to an average over 10 different simulations. During the adaptation period, the network was continually rewired once every  $T = 0.2$  time units. For high enough coupling, co-evolution results in a decrease of the number of synchronized clusters over time.

coupling  $\alpha$  (using mean degree  $\langle k \rangle = 25$  and uniformly distributed natural frequencies  $\{\omega_U\}$ ). We see that the number of synchronized clusters is initially large, since the oscillators' phases were distributed at random. Before the red line, the system evolves on a static ER network, and depending on the coupling strength, the number of components either fluctuates around a high value or - after an initial transient - rapidly decreases to a lower value, denoting partial synchronization. Network adaptation begins at the time denoted by the red line, after which the behavior of  $n_{sc}(t)$  is again determined by the global coupling. For very low  $\alpha$ , the co-evolution process does not significantly affect the number of synchronized clusters. However, as the coupling increases, the network rewiring begins to have an impact on the dynamical clustering. At intermediate  $\alpha$  values, the number of synchronized components slowly decreases as a function of time. For higher coupling values, this transition takes place more rapidly. However, it appears that no matter the coupling regime, the transition from high to lower  $n_{sc}$  does not occur abruptly at a single instance of time, but instead occurs over several time steps through the merging of clusters. In addition to the individual curves of the number of synchronized clusters vs. time, Fig. 2 depicts averages of  $n_{sc}(t)$  vs.  $t$  over 10 simulations using different instantiations of the initial conditions.

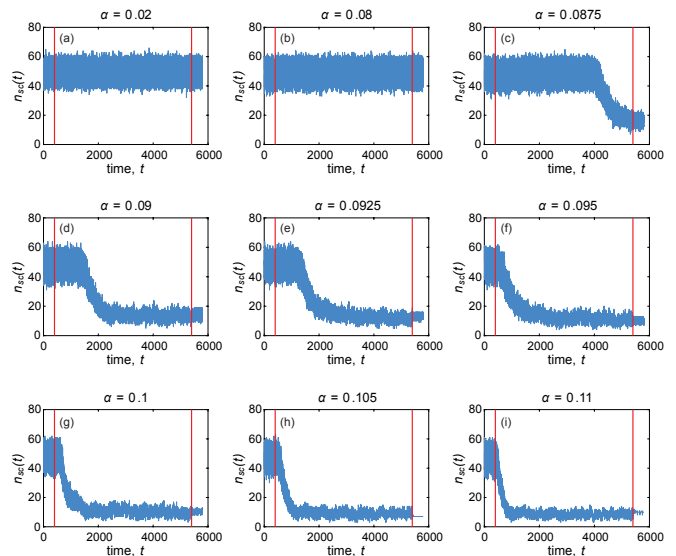


FIG. 3. Examples of the number of synchronized clusters  $n_{sc}(t)$  vs. time  $t$ , for various representative couplings  $\alpha$ . In each case, the dynamics were first run atop an initially ER random graph, after which co-evolution of the network and dynamics took place between the two red lines. For these plots, the natural frequencies were drawn from the normal distribution  $\{\omega_G\}$  and the mean degree of the network was  $\langle k \rangle = 12.5$ . During the adaptation period, the network was continually rewired once every  $T = 0.2$  time units. For high enough coupling, co-evolution results in a decrease of the number of synchronized clusters over time.

Fig. 3 and Fig. 4 show shows  $n_{sc}(t)$  vs. time  $t$  and the averages  $\bar{n}_{sc}(t)$  vs.  $t$ , respectively, for the case of mean degree  $\langle k \rangle = 12.5$  and normally distributed natural frequencies  $\{\omega_G\}$ . We find similar results to those for the denser networks. At low values of the coupling, network adaptation does not cause a consistent change in  $n_{sc}$ . As the coupling increases, however, the number of components begins to decrease from its initial value, signifying the merging or growth of synchronized clusters due to rearrangements in the network. This decrease becomes more rapid at larger couplings, though does not occur discontinuously as a function of time.

## II. VARIATION OF NETWORK SIZE, INITIAL NETWORK TOPOLOGY, AND FREQUENCY DISTRIBUTION

In the main text (and Appendix), we fixed the system size to be  $N = 100$  and initialized the networks as ER random graphs with mean degree  $\langle k \rangle = 25$  or  $\langle k \rangle = 12.5$ . We then examined two symmetric distributions (uniform and normal) for the intrinsic frequencies of the oscillators. In this section, we explore the robustness of certain results to some simple variations of the network size, the initial network topology, and the frequency distribution.

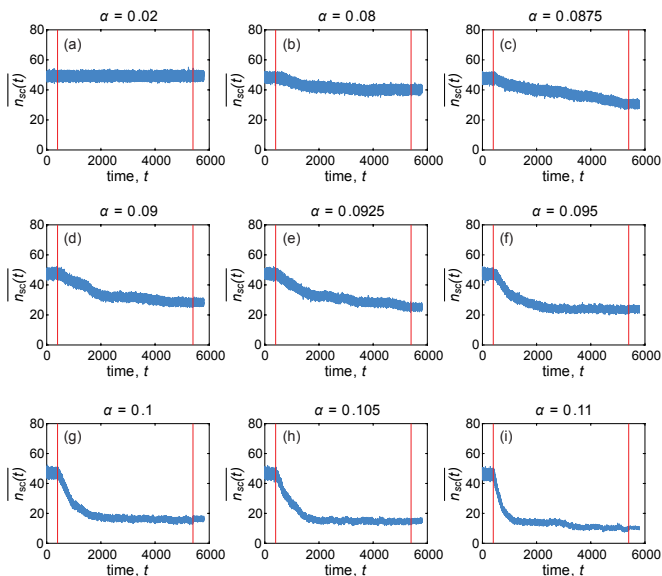


FIG. 4. Ensemble averages of the number of synchronized clusters  $n_{sc}(t)$  vs. time  $t$ , for various representative couplings  $\alpha$ . In each case, the dynamics were first run atop an initially ER random graph, after which co-evolution of the network and dynamics took place between the two red lines. For these plots, the natural frequencies were drawn from the normal distribution  $\{\omega_G\}$ , the mean degree of the network was  $\langle k \rangle = 12.5$ , and each curve corresponds to an average over 10 different simulations. During the adaptation period, the network was continually rewired once every  $T = 0.2$  time units. For high enough coupling, co-evolution results in a decrease of the number of synchronized clusters over time.

### A. Larger networks

We first investigate the effect of the co-evolutionary mechanism on the degree of synchronization for a doubling of the network size to  $N = 200$  (while also proportionately doubling the number of rewirings allowed for the adaptation process). Fig. 5a shows the order parameter  $\langle R \rangle$  vs. coupling  $\alpha$  for the case of uniformly distributed frequencies  $\{\omega_U\}$ , mean degree  $\langle k \rangle = 25$ , and a rewiring time scale of  $T = 0.2$  time units. We find qualitatively similar results to that of  $N = 100$  (Fig. 3b of the main text), in that the curve corresponding to the adapted networks (blue) is shifted to the left compared to the curve corresponding to a set of static, random ER networks (gray). Thus, over a large range of global coupling, the co-evolved networks exhibit a heightened degree of collective dynamics. Although the main contribution of the current work has been to suggest a local, dynamic rewiring mechanism for obtaining enhanced synchrony in conjunction with interesting dynamical and topological relationships - and an in-depth examination of the effect of system size is beyond the scope of this study - it is important that the results are consistent for a somewhat larger system size. We refer the reader to [2] for a detailed finite-size study and analysis of the critical

coupling and critical exponents in oscillator populations with purposefully constructed correlations.

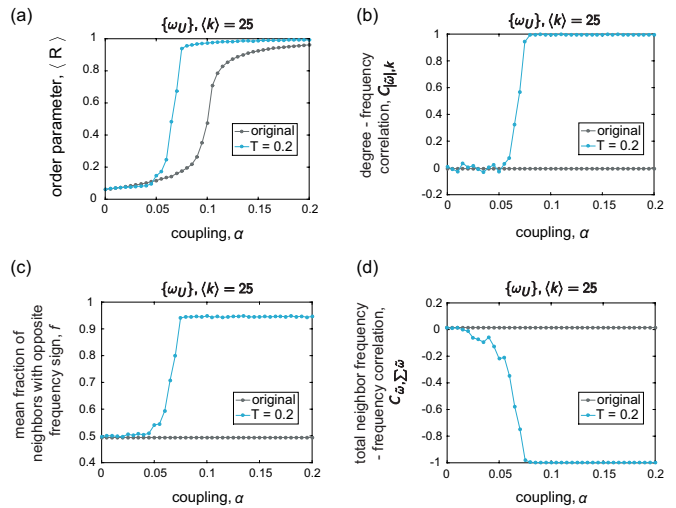


FIG. 5. Analysis of synchronization and emerging correlations for networks of size  $N = 200$  nodes. In each panel, the gray data points correspond to the initial ER networks  $\mathcal{G}_o$  with mean degree  $\langle k \rangle = 25$ , and the blue points correspond to the adapted networks  $\mathcal{G}_*$  evolved under a rewiring time scale of  $T = 0.2$  time units. The natural frequencies were drawn from the uniform distribution  $\{\omega_U\}$ . (a) The time-averaged order parameter vs. coupling. (b) The correlation  $C_{|\tilde{\omega}|,k}$  between node degree  $k_i$  and the magnitude of the frequency offset  $|\tilde{\omega}_i|$ , as a function of the coupling. (c) The mean fraction  $f$  of an oscillator's neighbors that have frequency offsets of opposite sign compared to the given oscillator, as a function of the coupling. (d) The correlation  $C_{\tilde{\omega}, \sum \tilde{\omega}}$  between oscillator frequency offset  $\tilde{\omega}_i$  and the sum of neighbor frequency offsets  $\sum \tilde{\omega}_j$ , as a function of the coupling. All curves depict averages over 10 instantiations, and the lines between data points serve as guides for the eye.

In addition to the order parameter, we also assessed the co-evolved networks  $\mathcal{G}_*$  for the emergence of correlations between their topology and the intrinsic frequencies of the oscillators (as done in Sec. IV B of the main text). The results of this analysis are shown in Fig. 5(b - d). As found previously for the case of  $N = 100$ , we find that the same set of relationships appear when the system size is doubled. Following the analysis described in the main text, for each node  $i$ , we compute its offset from the mean frequency  $\tilde{\omega}_i = \omega_i - \langle \omega \rangle$ , where  $\langle \omega \rangle$  is the mean natural frequency of the population. We then consider correlations between  $|\tilde{\omega}_i|$  and node degree  $k_i$  (panel (b)), and between  $\tilde{\omega}_i$  and the total neighbor frequency offset  $\sum \tilde{\omega}_j$  ( $\forall j \in \mathcal{N}(i)$ ) (panel (d)). In addition, we compute the fraction of an oscillator's neighbors  $f_i$  that have a value of  $\tilde{\omega}$  of opposite sign to that of  $\tilde{\omega}_i$ , and then compute the average  $f$  over all components in the network (panel (c)). As the coupling increases, there is an increasingly positive correlation  $C_{|\tilde{\omega}|,k}$  between degree and the magnitude of the intrinsic frequency offset, and an increasingly negative correlation  $C_{\tilde{\omega}, \sum \tilde{\omega}}$  between the intrinsic frequency

offset of each oscillator and the sum of its neighbors' frequency offsets. Furthermore, oscillators tend to become surrounded by other oscillators that have intrinsic frequency offsets on the opposite side of the mean.

## B. Smaller mean degree

This study has focused on networks with relatively large mean degree (yielding density values similar to that of large-scale human brain structural networks, for example [3], but many other real-world systems - such as social networks [4] - are more sparsely connected. Here, we thus briefly examine whether the results hold for networks with a lower mean degree of  $\langle k \rangle = 6$ . Fig. 6a shows the time-averaged order parameter  $\langle R \rangle$  vs. coupling  $\alpha$  for the initial, static ER networks (gray curve) and the adapted networks (blue curve). The parameters used were uniformly distributed frequencies  $\{\omega\} = \{\omega_U\}$ , mean degree  $\langle k \rangle = 6$ , and a rewiring time scale of  $T = 0.2$  time units. As for the denser networks considered in the main text, here we also observe a significant enhancement of the order parameter for the co-evolved systems.

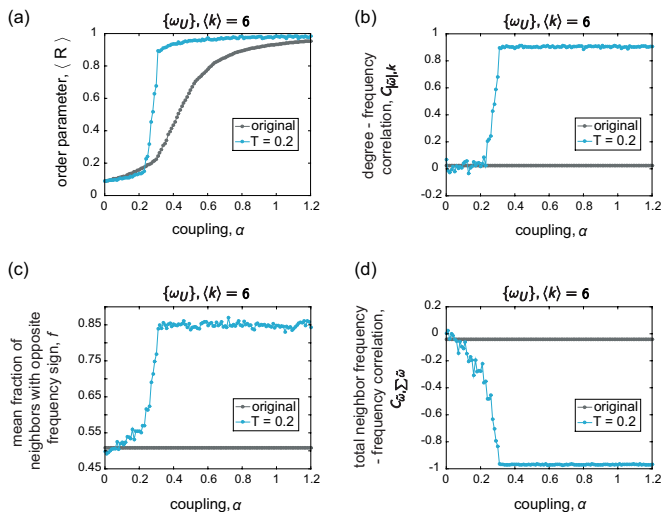


FIG. 6. Analysis of synchronization and emerging correlations for networks with sparser connectivity. In each panel, the gray data points correspond to the initial ER networks  $\mathcal{G}_o$  with mean degree  $\langle k \rangle = 6$ , and the blue points correspond to the adapted networks  $\mathcal{G}_*$  evolved under a rewiring time scale of  $T = 0.2$  time units. The natural frequencies were drawn from the uniform distribution  $\{\omega_U\}$ . (a) The time-averaged order parameter vs. coupling. (b) The correlation  $C_{|k|,k}$  between node degree  $k_i$  and the magnitude of the frequency offset  $|\tilde{\omega}_i|$ , as a function of the coupling. (c) The mean fraction  $f$  of an oscillator's neighbors that have frequency offsets of opposite sign compared to that of the given oscillator, as a function of the coupling. (d) The correlation  $C_{\sum \tilde{\omega}}$  between oscillator frequency offset  $\tilde{\omega}_i$  and the sum of neighbor frequency offsets  $\sum \tilde{\omega}_j$ , as a function of the coupling. All curves depict averages over 10 instantiations, and the lines between data points serve as guides for the eye.

We also examined the locally adapted networks for the same set of emergent relationships between dynamical properties (natural frequencies) and topological organization. Fig. 6 panels (b-d) then show  $C_{|k|,k}$ ,  $f$ , and  $C_{\sum \tilde{\omega}}$ , respectively, as a function of the coupling. We find that as the coupling increases, there is an increasingly positive correlation between degree and the magnitude of intrinsic frequency offset, and an increasingly negative correlation between the intrinsic frequency offset of an oscillator and the sum of its neighbors' frequency offsets. Furthermore, oscillators tend to become surrounded by other nodes with frequency offset on the opposite side of the mean. Although the curves shown here for the case of  $\langle k \rangle = 6$  exhibit somewhat more fluctuations compared to the case  $\langle k \rangle = 25$ , the findings are in general robust and consistent with those found for networks with higher mean degree.

## C. Initial network topology

modular - small world network,  $\langle k \rangle = 20$

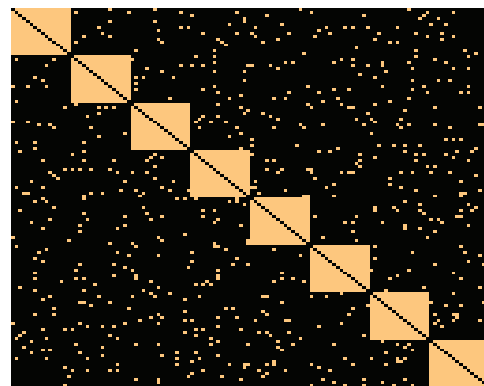


FIG. 7. An example of the connection pattern of a modular - small world network of size  $N = 128$ , with 8 communities and a mean degree  $\langle k \rangle = 20$ .

The main interest and goal of this paper has been to define and explore a simple, local mechanism that evolves some initial network of coupled oscillators to a structured configuration that in turn supports enhanced collective dynamics. Given this objective, ER random graphs - which are considered to be relatively "disordered" - are a natural family of networks on which to begin the co-evolution and against which to compare the adapted systems. However, it may still be useful to examine if the results hold for a different starting network topology. To test this, we constructed a set of modular - small world (MSW) networks, which consist of a specified number of fully connected communities that are then linked together by placing edges at random between modules. In contrast to the ER random graph model, these networks contain a significant amount of planted structure. For this analysis, we used networks of size  $N = 128$ , with

$N_c = 8$  modules, and a total number of edges such that the average degree was  $\langle k \rangle = 20$ . Fig. 7 shows an example connection pattern.

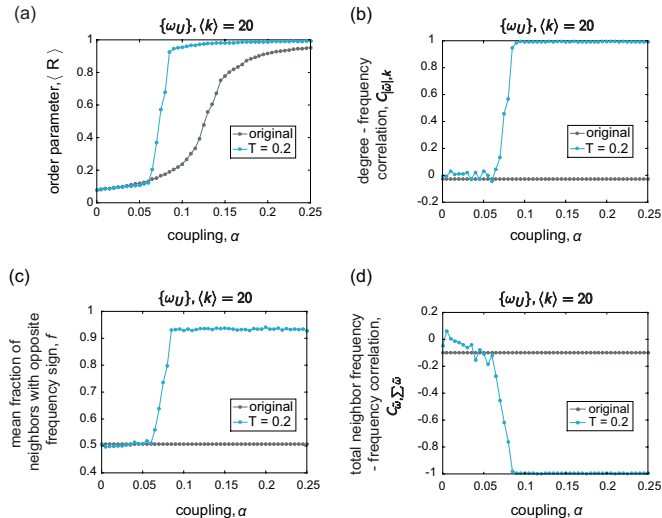


FIG. 8. Analysis of synchronization and emerging correlations when the initial network topology is modular-small world, rather than a random graph. In each panel, the gray data points correspond to the initial MSW networks  $\mathcal{G}_o$  (see text for the parameters used), and the blue points correspond to the adapted networks  $G_*$  evolved under a rewiring time scale of  $T = 0.2$  time units. The natural frequencies were drawn from the uniform distribution  $\{\omega_U\}$ . (a) The time-averaged order parameter *vs.* coupling. (b) The correlation  $C_{|\tilde{\omega}_i|,k}$  between node degree  $k_i$  and the magnitude of the frequency offset  $|\tilde{\omega}_i|$ , as a function of the coupling. (c) The mean fraction  $f$  of an oscillator's neighbors that have frequency offsets of opposite sign compared to the given oscillator, as a function of the coupling. (d) The correlation  $C_{\tilde{\omega}_i, \sum \tilde{\omega}_j}$  between oscillator frequency offset  $\tilde{\omega}_i$  and the sum of neighbor frequency offsets  $\sum \tilde{\omega}_j$ , as a function of the coupling. All curves depict averages over 10 instantiations, and the lines between data points serve as guides for the eye.

Due to the nature of the adaptive mechanism, we expect that it will undo the seeded community structure and still evolve this class of networks towards topologies with the same set of features we have discussed thus far. To test the validity of this expectation, we first simulated the Kuramoto dynamics on non-adaptive MSW networks, and then used the same set of MSW networks as the initial network configurations for the adaptive mechanism. Fig. 8a shows the time-averaged order parameter  $\langle R \rangle$  *vs.* coupling  $\alpha$  for the case of uniformly distributed frequencies  $\{\omega_U\}$ , and a rewiring time scale of  $T = 0.2$  time units. The adaptively rewired networks (blue curve) show heightened global synchronization across a large range of coupling values compared to the static MSW networks (gray curve). Turning next to the correlations between the natural frequencies and the network organization, we find results consistent with those described in the main text. (See Fig. 8b - d for plots of  $C_{|\tilde{\omega}_i|,k}$ ,  $f$ , and  $C_{\tilde{\omega}_i, \sum \tilde{\omega}_j}$ , respectively). In particular, strong degree -

frequency correlations and frequency - neighbor frequency mixing emerge in the self-organized systems. This investigation provides some evidence that the adaptive mechanism is agnostic to the initial network configuration from which it begins.

#### D. Natural frequency distribution

One could also explore the dependence of results on the natural frequencies. We considered two standard distributions - uniform and normal - that are often used in studies on the Kuramoto model. Here, we show some brief additional results for the case of natural frequencies  $\{\omega_P\}$  drawn from a power-law distribution in which  $P(\omega) \propto \omega^{-\gamma}$ , with  $\gamma = 3$ . The dynamics and network co-evolution start from ER random graphs with  $N = 200$  nodes and mean degree  $\langle k \rangle = 25$ . We find similar results for the adaptive rewiring scheme when using this skewed distribution for the intrinsic frequencies.

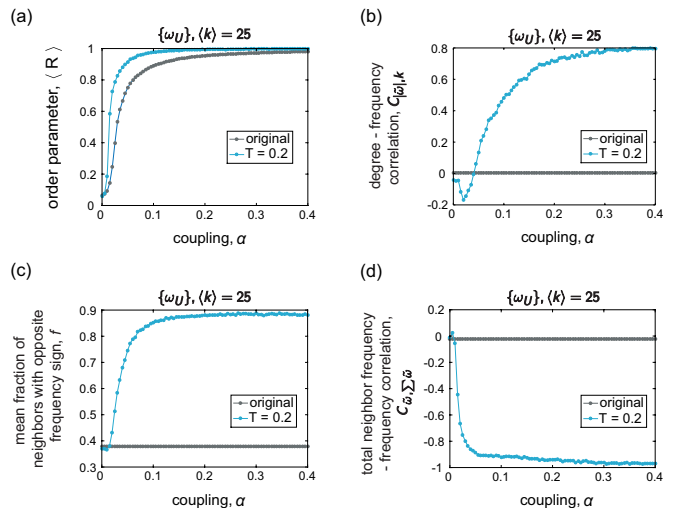


FIG. 9. Analysis of synchronization and emerging correlations when the natural frequencies are drawn from a power law distribution with exponent  $\gamma = 3$ . In each panel, the gray data points correspond to the initial ER networks  $\mathcal{G}_o$  (see text for the parameters used), and the blue points correspond to the adapted networks  $G_*$  evolved under a rewiring time scale of  $T = 0.2$  time units. The network size is  $N = 200$ . (a) The time-averaged order parameter *vs.* coupling. (b) The correlation  $C_{|\tilde{\omega}_i|,k}$  between node degree  $k_i$  and the magnitude of the frequency offset  $|\tilde{\omega}_i|$ . (c) The mean fraction  $f$  of an oscillator's neighbors that have frequency offsets of opposite sign compared to the given oscillator, as a function of the coupling. (d) The correlation  $C_{\tilde{\omega}_i, \sum \tilde{\omega}_j}$  between oscillator frequency offset  $\tilde{\omega}_i$  and the sum of neighbor frequency offsets  $\sum \tilde{\omega}_j$ , as a function of the coupling. All curves depict averages over 10 instantiations, and the lines between data points serve as guides for the eye.

Fig. 9 shows the time-averaged order parameter  $\langle R \rangle$  *vs.* coupling  $\alpha$  for the static ER networks (gray curve) and adaptively rewired networks (blue curve). The rewiring

time scale was  $T = 0.2$  time units. As with the two symmetric frequency distributions, we observe an increase in the order parameter for the networks evolved according to the local mechanism. We also examined the co-evolved networks  $G_*$  for the correlations between natu-

ral frequency offsets and the topological organization of the network. Fig. 9*b - d* show plots of  $C_{|\tilde{\omega}|,k}$ ,  $f$ , and  $C_{\tilde{\omega},\Sigma_{\tilde{\omega}}}$ , respectively. Consistent with the results in the main text, we observe the emergence of strong degree-frequency correlations and frequency-neighbor frequency mixing patterns.

- 
- [1] A. Arenas, A. Díaz-Guilera, and C. J. Pérez-Vicente, Phys. Rev. Lett. **96**, 114102 (2006).  
 [2] M. Brede, Physica D: Nonlinear Phenomena **239**, 1759 (2010).  
 [3] D. S. Bassett, J. A. Brown, V. Deshpande, J. M. Carlson, and S. T. Grafton, Neuroimage **54**, 1262 (2011).  
 [4] M. E. J. Newman, SIAM Review **45**, 167 (2003).